The International Journal of Advanced Manufacturing Technology (2018) 99:1427–1448
https://doi.org/10.1007/s00170-018-2563-z

ORIGINAL ARTICLE

Review on intermittent local loading forming of large-size complicated component: deformation characteristics

Da-Wei Zhang [1] · Xiao-Guang Fan [2]

Received: 1 February 2018 / Accepted: 13 August 2018 / Published online: 22 August 2018

Abstract

Intermittent local loading forming is an important aspect of less-force plastic forming technologies. It has many advantages such as high flexibility of the forming process, multiplicity of loading way, and multiple controllable degree of freedom, and thus it shows a good prospect of application in plastic forming for an irregular integral component with a large-size and complicated structure, such as the large-size rib-web integral component. Up to now, the intermittent local loading methods used to manufacture a large-size complicated component can be classified into three categories such as local loading by simple punch, local loading by bolster plate, and local loading by partial die. The state-of-art of three local loading processes was summarized from four aspects such as actualization in industry of local loading process, loading state and metal flow during local loading process, influence of friction on local loading process, and defect and control during local loading process.

Keywords Bulk forming · Intermittent local loading · Less-force forming · Large-size complicated forging · Rib-web component

1 Introduction

With the rapid development of aviation, aerospace, and machinery industries, the demands of performance, reliability, and lightweight for components are increasing, and then the components develop towards large-size integration, complex thin-wall, and making by lightweight material with hard-to-deform feature [1–5]. Many of these components are rib-web components, and their materials are mainly aluminum alloy, magnesium alloy, and titanium alloy. However, these large-size integrated components have a complicated structure, large plan view, and hard-to-deform metal. Thus, the traditional whole forging process needs heavy load and the load goes beyond the capability of equipment. However, the local loading process can reduce forging load and expand capability of equipment.

According to continuities of plastic deformation in space and time, the local loading forming processes of bulk forming fall into continuous local loading and intermittent local loading. During the forming cycle of continuous local loading process, the die (or dies) keeps contact with the workpiece, and there exists one or more fixed or continuous changed local deformation zone in space. The representative processes are cross-wedge rolling [6], roll-forging [7], ring rolling [8], rotary forging [9], spinning [10], thread rolling [11], etc. However, the die (or dies) contacts with the workpiece intermittently during the intermittent local loading process, and the contact and separate between the die (or dies) and workpiece happen repeatedly. The representative processes are radial forging [12], rotary swaging [13], open-die forging (or named free forging) [14, 15], incremental forging [16], spline rolling [17], etc.

The intermittent local loading forming technology presents high flexibility of forming process, and multiple controllable degree of freedom for loading approach. Thus, intermittent local loading forming technology shows a good prospect of application in plastic forming for an irregular integral component with large-size and complex structure. It is more suitable to manufacture an asymmetric and irregular integral component, such as large-size integral component with high rib and thin web.

✉ Da-Wei Zhang
zhangdawei2000@mail.xjtu.edu.cn; zhangdawei2000@xjtu.edu.cn

[1] Key Laboratory of Education Ministry for Modern Design and Rotor-Bearing System, School of Mechanical Engineering, Xi'an Jiaotong University, No.28, Xianning West Road, Xi'an 710049, Shaanxi, People's Republic of China

[2] State Key Lab of Solidification Processing, School of Materials Science and Engineering, Northwestern Polytechnical University, 710072 Xi'an, People's Republic of China

Since the 1960s, improvement and innovation for the local loading process have been implemented to break through the capability of equipment and to manufacture large-size complicated component. With the development of forming technology, the physical dimension of forging becomes larger and larger, and the shape of forging becomes more and more complex. Up to now, the intermittent local loading methods to manufacture a large-size complicated component can be classified into three categories according to the publications, such as local loading by simple punch (LLbSP), local loading by bolster plate (LLbBP), and local loading by partial die (LLbPD) [18, 19].

Some reviews on deformation characteristics of local loading process have been reported [20–22], but it did not involve the above three types of intermittent local loading process. The local loading by dividing the upper die into several parts was shortly introduced in the reviewing articles [4, 23]. References [24, 25] summarized some features of local loading by partial die mentioned above. However, some new features were explored and many new publications were published in recent years. Thus, in this paper, the technical principles of three intermittent local loading methods for large-size complicated component were summarized, and their applications and manufacture of type of components were reviewed, and the state-of-art of deformation characteristics in local loading process was presented. It provides a fundamental and applicability of local loading process of large-size complicated component.

2 Local loading method and its actualization in industry

Three local loading methods to manufacture large-size complicated component will be introduced in the following sections. The first method is local loading by simple punch, the second method is local loading by bolster plate, and the third method is local loading by partial die. For some complicated components made by material with narrow processing window, the local loading process will combine with isothermal forging.

2.1 Local loading by simple punch (LLbSP)

The upper die is replaced by small simple punch for local loading by simple punch. During local loading process by simple punch, only the metal under the simple punch is loaded, and the local plastic deformation is accumulated, and then the integral component is formed. Compared with the other two local loading methods, the shape of component formed by this local loading method is relatively simple.

In 1960s, Скородюмов presented an increment forging technology to manufacture large forging of titanium alloy in order to solve the problem of inadequate capability of the hydraulic press [26]. Then, Abramowitz and Sokey investigated the feasibility of small batch die forging by increment forging, where the rib-web component was adopted as a research object [26]. They declared that the increment forging technology is suitable to manufacture preform or simple-shape forging.

The Institute for Metal Forming (Aachen University of Technology) studied the flexile intermittent local loading technology since the 1980s [27, 28]. Finally, a local loading forming process was developed as follows: the simple punch is controlled accurately to load in local area, and then metal flows to form rib. Three classes of local loading method can be available [16], as shown in Fig. 1, and several loading passes can be adopted to obtain the required rib height.

An aluminum alloy component (360mm × 360mm) with ribs on one side was formed by using local loading method shown in Fig. 1b, and 30% of material is saved, and the forming load is only 10% of the load by using the whole loading process [27, 28]. The simple punch should be positioned accurately and forged quickly, so it needs a special type of press to meet these requirements [16]. Thus, the fuzzy control and robot were introduced into the forging machine [29]. The simple punch developed into four series such as round,

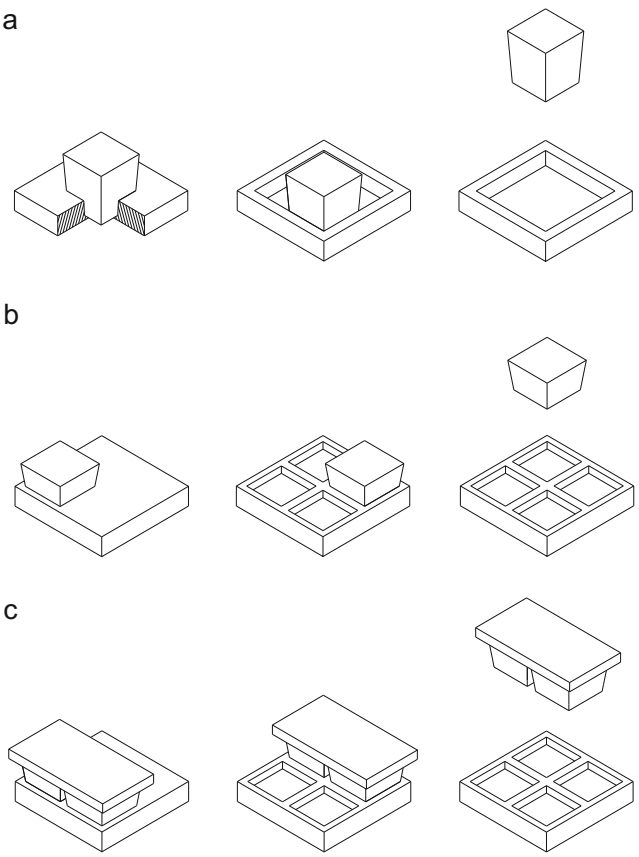

Fig. 1 Principle of local loading using standard elementary dies: **a** first process, **b** second process, and **c** third process

square, rectangular, and triangular after standardizing and serializing. The integral rib-web component was manufactured by this local loading method with the combination of punch series, and 45% of material is saved compared with the whole machined component [16].

A less-force forming process for large Cu-lids was developed in the study [30], where a bar punch is used to load locally. The forming process includes two operations: whole loading operation, as shown in Fig. 2a, the peripheral ring rib-cavity is under-filling after this operation, and local loading operation, bar punch is applied to the peripheral local area at first, and then to the diagonal local area, as shown in Fig. 2b, and finally, the rib-cavity is filled completely. The lid with 500 mm in diameter was formed with max 4600 t, but traditional whole forging needs 25,000 t.

2.2 Local loading by bolster plate (LLbBP)

The intermediate auxiliary operation, such as a bolster plate being placed between the upper die and billet, is used to realize local loading for local loading by bolster plate. Some different bolster plates are adopted at different forming stages according to the structure of the component, where only the metal under the bolster plate is loaded when the upper die presses.

In order to reduce the contact area, the bolster plate was placed between the upper die and billet by Lü et al. [31–33]. Then, the isothermal local loading process for magnesium alloy upper housing was implemented. They declared that the local loading area and shape of the local loading tool (i.e., bolster plate) should be considered together to be smooth transition between different deformed zones. The process includes several stages, and different bolster plates (Fig. 3a) were used, respectively. The cavity filling was improved and the forming load was decreased by 70%. Figure 3b illustrates the formed forging with 680 mm in diameter.

Based on these, transitive die plate and annular bolster plate were adopted by Shan et al. [34–36] to realize local loading. An aluminum alloy hatch with cross ribs on one side was manufactured by using this method of local loading combined with isothermal forging. The whole loading and local loading were alternated during the process, and the transitive die plate (Fig. 4a) and annular bolster plate (Fig. 4b) were repeatedly replaced. During the process, the metal is gathered at the opposite side of rib cavity by using transitive die plate, and stress state is changed by using an annular bolster plate. So the fill can be improved and the folding can be avoided, and the good forging of aluminum alloy hatch can be obtained, as shown in Fig. 4c, which was 500 mm in length and 400 mm in width.

A titanium alloy forging with 360 mm in diameter and 5 in ratio of rib height to width was manufactured by this local loading method [37]. Where, the local loading is carried by using a bolster plate at first, and then whole loading is carried out after taking out the bolster plate. The folding and flow lines disturbance in the whole loading process were avoided by the local loading. And the material utilization increased from 34% in traditional whole forging to about 80% in hot forging with local loading.

It is not mentioned that there are some special requirements for the press by using this local loading method. The formed surface of the component contacting with the bolster plate has a simple shape, and generally is a machined surface. The local loading method by bolster plate is also suitable for manufacturing a component with ribs on one side. The formed components mentioned above are with rib on one side.

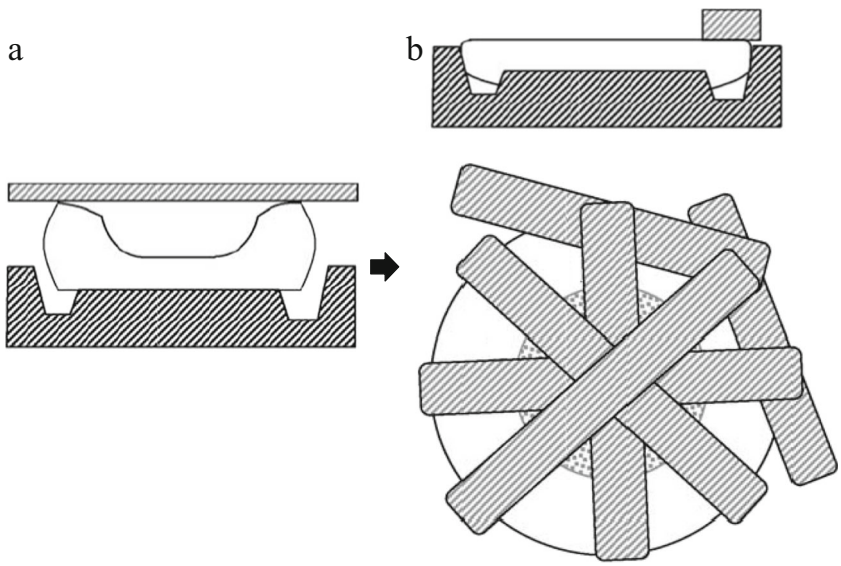

Fig. 2 Workpiece geometry and forming sequences [30]: **a** whole loading and **b** local loading

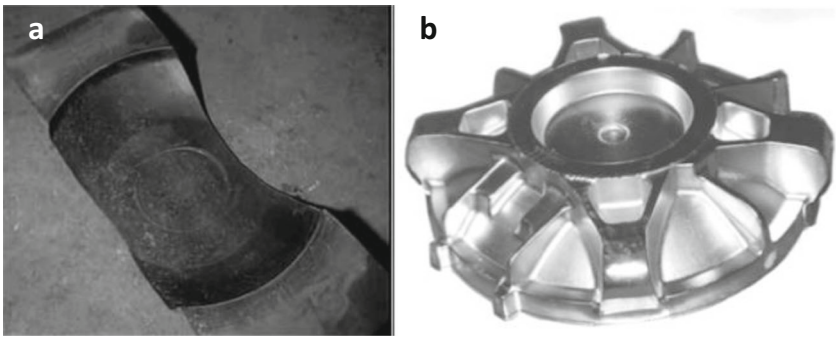

Fig. 3 Magnesium alloy upper housing manufactured by local loading method [33]: **a** bolster plate and **b** forging

2.3 Local loading by partial die (LLbPD)

During the local loading process by the partial die, only the partial die is loaded in the local loading step; the integral component is formed by the coordination and accumulation of local plastic deformation. Generally, one or several loading passes are adopted according to total deformation, and two or more local loading steps are adopted in one loading pass according to the capability of the equipment. Compared with the above two local loading methods (LLbSP and LLbBP), the processing concept of local loading by partial die is simple, and its loading path/route is also simple. The large-size component with complex shape on both sides can be formed by this local loading method.

2.3.1 Manufacture of axisymmetric component

The technology of local loading by partial die is developed to manufacture an axisymmetric component at first. According to the geometric characteristic of the axisymmetric component, a partial upper die and a whole lower die are adopted. Only part of billet yields and deforms in the local loading step, and then the upper die or lower die rotates by a certain angle before the next local loading step, as shown in Fig. 5, to repeat loading and rotating until the desired shape is obtained. The partial upper die may be bar, fan-shaped, or other shape, where the plan view of the die is determined by the capability of the equipment.

In the 1970s, the local loading method and corresponding equipment were explored to manufacture a larger axisymmetric component under the then hydraulic press [38, 39]. The process, die, and equipment for this rotationally local loading were perfected in the 1990s [40].

Some industrial cases have been reported in China since 2000. A large integral container head was formed by this local loading method, and the diameter by local loading is 1.5 times the diameter by whole loading under the same hydraulic press [41]. The disks with over 1000 mm in diameter for steam turbine impeller were manufactured by this local loading method on a 630-kJ hammer [42]. The wheel disk and shroud disk of the fan impeller were also manufactured by this local loading method on a 2000-t hydraulic press [43], where diameters of which are more than 1200 mm. Figure 6 illustrates the formed forging of the shroud disk made by FV520B stainless steel.

2.3.2 Manufacture of non-axisymmetric component

For local loading technology for non-axisymmetric component, the integral upper or lower die is divided into several sub-dies. Only part (one or multi sub-dies) of the whole die is loaded in the local loading step, and to continually change the loading area in different local loading steps. The lower die was divided into several sub-dies to realize local loading in the study [44]. In order to implement on an isothermal forging hydraulic press, isothermal local loading way by dividing the upper die was developed by Yang's group [4, 5]. Figure 7a illustrates the forming principle developed by Yang et al., where two loading passes and three local loading steps in one pass are illustrated in the figure. A large-size

Fig. 4 Aluminum alloy hatch manufactured by local loading method [36]: **a** transitive die plate, **b** annular bolster plate, and **c** forging

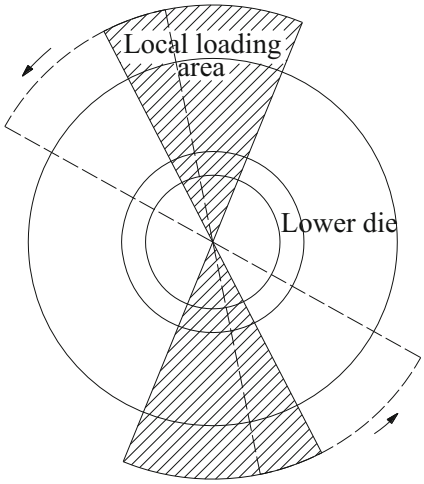

Fig. 5 Sketch of local loading by partial die with rotation

titanium alloy bulkhead with cross ribs on both sides was manufactured by the isothermal local loading process, as shown in Fig. 7b.

If the axial dimension of the component is much larger than the other two dimensions and cross section changes little along the axial direction, only one sub-die can be adopted, and the billet yields in sequence along the axial direction [45, 46], as shown in Fig. 8a. The form of local loading is similar to that in Fig. 1c, but the principle is different. During multi-passes local loading process by this method, the center of the loading upper die is positioned in the center of the region between two local loading areas in the last pass. The aluminum alloy forgings with 3700 mm [45] and 5000 mm [46] in length were manufactured by this method, as shown in Fig. 8b, c. The size of the formed component is much larger than the size of the workbench of the equipment.

The local loading way shown in Fig. 8a can be implemented on ordinary hydraulic press with axial motion of the workpiece. However, it needs some complex operations when the local loading way shown in Fig. 7a is implemented on the ordinary hydraulic press. Generally, there exist two approaches to actualize the local loading way by dividing the upper or lower die in industry, which are considered from the aspects of the equipment and the die, respectively. The former requires a special hydraulic press, and the latter can be carried out on an ordinary isothermal forging hydraulic press.

Fig. 6 Shroud disk manufactured by local loading with rotational partial die [43]

The special hydraulic press has two or more slide blocks (i.e., moving beams), and each slide block is run by its own hydraulic system (i.e., drive system), and each hydraulic system can provide enough forging force for deformation of the workpiece. Then, the sub-dies are attached to the different slide blocks, respectively, as shown in Fig. 9, so each sub-die can move discretionarily.

The local loading way also can be actualized in ordinary hydraulic press by means of adjusting the die structure and adding auxiliary device. In general, a spacer block is placed between loading sub-die(s) and corresponding die bed in order to support the loading sub-die(s) protruding out along forging axis, and then the loading sub-die(s) (i.e., protruded sub-die(s)) transfers the vast majority of forging force to the billet/workpiece, and the constraint is applied to other area of the billet by not loaded sub-die(s). When partition for the upper die, a spacer block is placed over the loading sub-die (i.e., upper die 1) in order to make it lower than the not loaded die (i.e., upper die 2), as shown in Fig. 10a; when partition for the lower die, a spacer block is placed under the loading sub-die in order to make it higher than the not loaded die.

During the local loading process shown in Fig. 9, the loading sequence and movement of each sub-die could be easily controlled, and then the loading region could be easily changed, and several local loading steps and loading passes could be implemented by one heating. However, it needs a type of hydraulic press with two or more main hydraulic systems both of which can provide a rather large forging force. However, the double-action press has one main hydraulic system and one auxiliary hydraulic system at present, in which the auxiliary hydraulic system only provides low deformation energy. In general, this double-action hydraulic press is usually used for sheet forming, and is not suitable for local loading forging shown in Fig. 9. A double-action hydraulic system was designed to solve the problems above [47], which has a capability of proving a larger energy than the installed power.

There exists no special requirement for hydraulic press by the way shown in Fig. 10, but it is difficult to adjust the position of the loading and not loaded dies. In order to adjust the position, it is unavoidable to remove the workpiece and cool the die after one local loading step, and then the sub-dies are repositioned before the next local loading step. However, it is based on the current hydraulic press and is prone to be used in industrial application. In general, one loading pass with two local loading steps is adopted to simplify the process. The reported industrial cases are both using this way [4, 44], for example, the formed component in Fig. 7b.

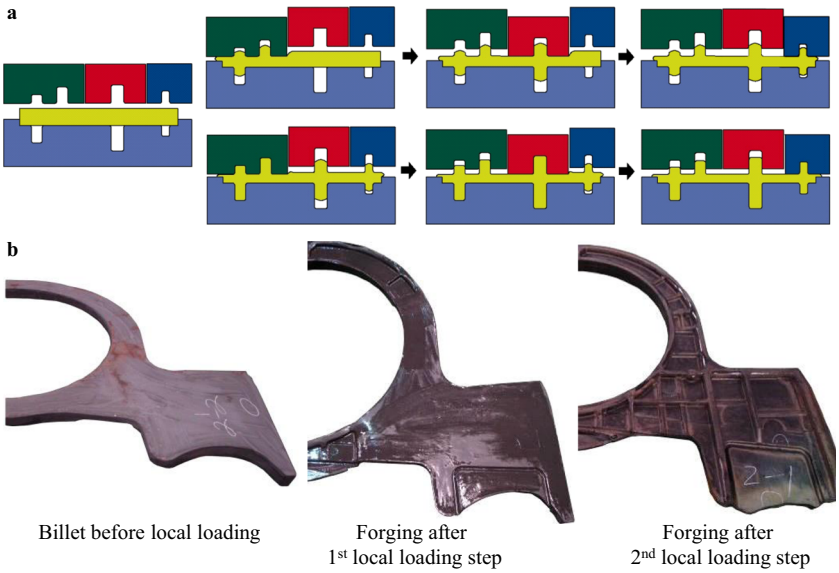

Fig. 7 Intermittent local loading technology of non-axisymmetric component: **a** sketch of forming principle [5] and **b** forging during local loading process [4]

3 Loading state and metal flow

The local loading methods presented in Section 2 are chiefly used in manufacture of a large-size rib-web component. Thus, the discussion in this section and following is concerned with the manufacture of a rib-web component.

For the local loading by bolster plate or partial die, the local loading presents from the overall situation at first. Thus, the local loading area near the boundary of the bolster plate or partial die has always been strongly focused. However, the whole loading state may appear from partial view, because of the large loading area with multi-cavity. The deformation behavior may be various due to the different local loading states. According to the geometric characteristic of billet and die, there are one whole loading state and three local loading states in the local loading process of large-size component [48], as shown in Fig. 11b–e.

In the local loading area during the local loading process, there is the zone between two filled cavities with zero or little stress in the loading direction, and this zone/boundary is defined as free boundary which is similar to that in the not loaded area. There is a free boundary between filled cavities in the local loading state, and there is no free boundary between filled cavities in whole loading. The first local loading state is caused by die partition, and it presents near the die partitioning boundary and edge of bolster plate, and it exists through the local loading process. The second loading state is caused by difference (Δt) of distance between billet and web cavity, and it will turn into whole loading when the Δt disappears.

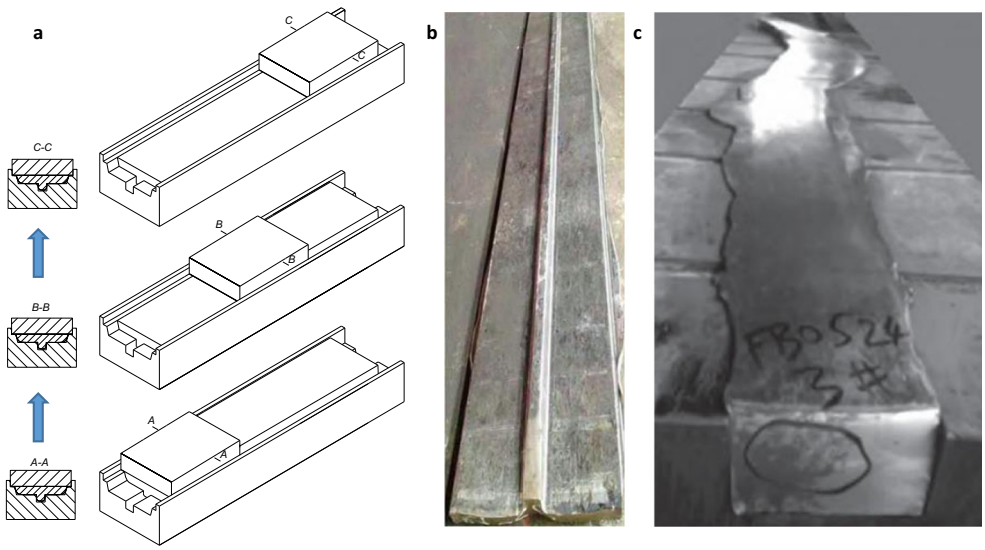

Fig. 8 Axial local loading by partial die: **a** sketch of forming principle, **b** T-shaped forging [45], and **c** aircraft forging [46]

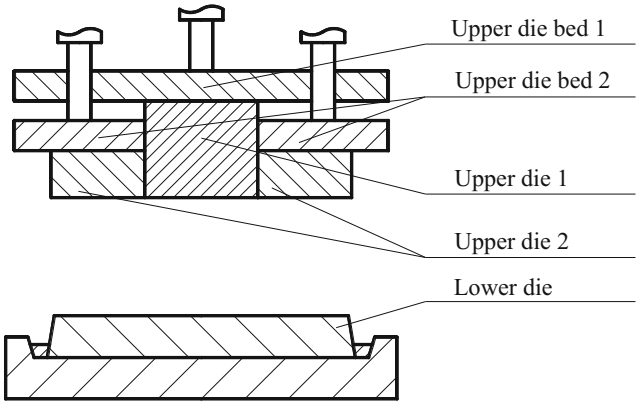

Fig. 9 Sketch of local loading in double-action hydraulic press (two slide blocks) [18]

The third local loading state is caused by thickness difference (ΔH) of billet, and it may present in the interior of the local loading area in the local loading process by bolster plate or by partial die, and it will turn into whole loading when the ΔH disappears. For example, this phenomenon appears in the local loading process by partial die with unequal-thickness billet (UTB) [48], and presents at the forming stage after gathering metal by transitive die plate in the local loading process by bolster plate [36].

According to the cause for the loading state, the three local loading states fall into two categories: the first and second local loading states are caused by geometric parameters of die (GPD), and the third local loading state is caused by geometric parameters of billet (GPB). Two local loading processes of T-shaped component were put forward and designed to reflect the local loading characteristic caused by GPD and GPB [49, 50], respectively, as shown in Fig. 11f, g.

Numerical [51, 52] and experimental [49] studies of the local loading process (shown in Fig. 11f) of T-shaped component were carried out to investigate the deformation behavior. The numerical results indicated that the upsetting-extrusion deformation will turn into shearing deformation with decreasing local loading width l. And the experimental results indicated that the shearing deformation will turn into upsetting-extrusion deformation with decreasing thickness of web in the loading area, but the shearing deformation dominates the through-process when the with l is less than a critical value. Thus, two simplified deformation patterns were established [49]: shearing deformation pattern, as shown in the left of Fig. 12a, where all the metal of web in the loading area flows towards the lateral portion (region II); upsetting-extrusion deformation pattern, as shown in the right of Fig. 12a, where part of metal of web in the loading area flows towards the lateral portion (region II) and the other metal flows into the cavity (region III).

The similar characteristic also presents in the local loading process shown in Fig. 11g [50], as shown in Fig. 12b. The simple unequal-thickness billet can be divided into two layers, two simplified deformation patterns, such as shearing deformation pattern and upsetting-extrusion deformation pattern, also present in layer 1, as shown in Fig. 12b. But the boundary condition from the not loaded area is different from that in the local loading state caused by GPD, and the distribution of metal flowing towards the lateral portion is also different. In the third local loading state, i.e., state caused by GPB, the local loading l dynamically changes and is lengthened by the part of metal flowing towards the lateral portion, and the thickness of layer 2 is thickened by the other metal flowing outward.

Analytical description of metal flow, such as the description using slab method (SM), has a clear physical insight and parametric relationship, and is helpful to explore the difference between different loading states. The analytical models for the whole loading state and local loading states were discussed in the studies [48–50], respectively.

In the whole loading state, the position (x_k) of neutral layer is at the medium position between two rib cavities; the SM model of x_k can be expressed as follows [48]:

$$x_k = \frac{1}{4}(l + b_i - b_{i+1}) + \frac{H^2}{4m}\left(\frac{1}{b_{i+1}} - \frac{1}{b_i}\right) \quad (1)$$

where $l = 2a_{i,\,i+1}$, $a_{i,\,i+1}$is the distance between rib i and rib $i+1$; $b_i$is the width of rib i; $b_{i+1}$is the width of rib $i+1$; H is the thickness of the web in the loading area; and m is the shear friction factor.

Metal within the width of x_k flows into the cavity of rib i, and the metal beyond the width of x_k flows into the cavity of rib $i+1$. There is only one deformation pattern similar to upsetting-extrusion deformation. If both widths of rib are the same, the x_k is half the distance between two ribs in the

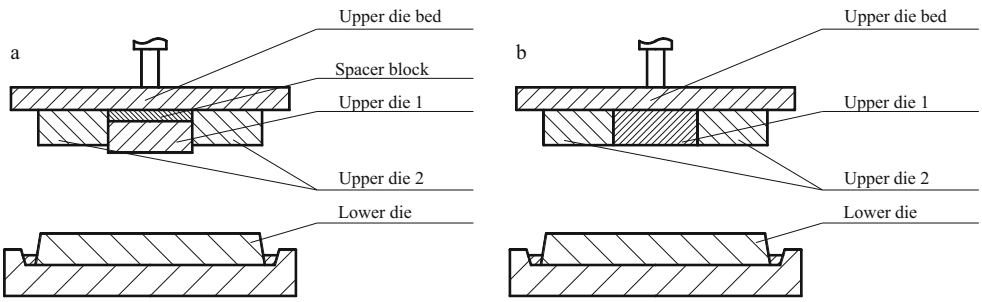

Fig. 10 Sketch of local loading in ordinary hydraulic press [18]: **a** the first two local loading step and **b** the second local loading step

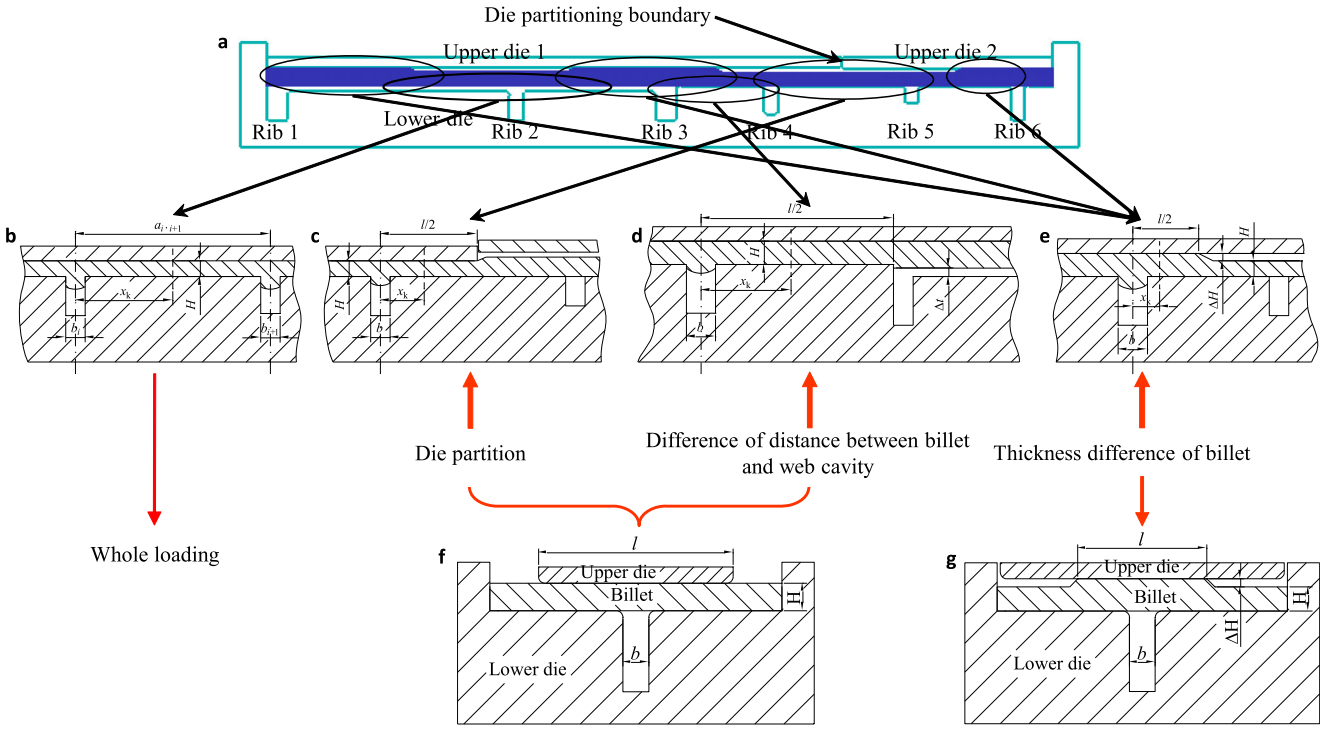

Fig. 11 Loading states in local loading process: **a** local loading process, **b** whole loading state, **c** first local loading state, **d** second loading state, **e** third local loading state, **f** eigenstructure reflects forming characteristic caused by GPD, and g eigenstructure reflects forming characteristic caused by GPB

through forming process. If both widths of rib are different, the x_k changes with the change of H in the forming process, and rib cavity with large width will be filled with more metal.

Three local loading states fall into two categories, and the metal flow characteristics can be expressed as Eq. (2) in the local loading state caused by GPD [49] and expressed as

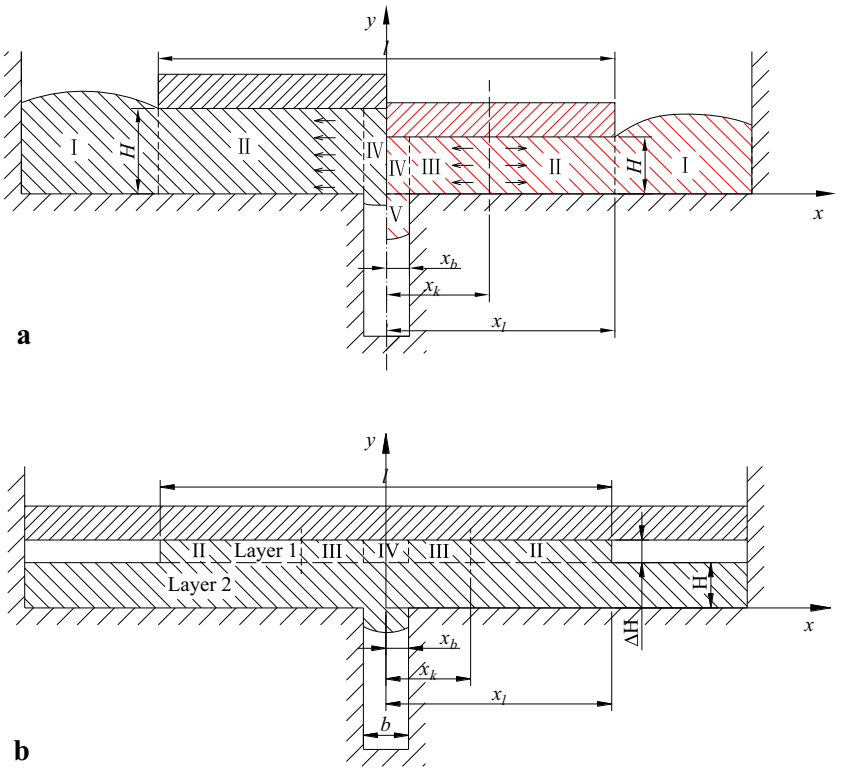

Fig. 12 Deformation pattern in local loading state caused by **a** GPD and **b** GPB

Eq. (3) in the local loading state caused by GPB [50], respectively. The SM models can properly describe the metal flow in the local loading state when $l/b > 5$, and predicted error decrease with increasing width of local loading [49, 50].

$$\begin{cases} x_k = \dfrac{b}{2} & \sigma_x^{II}\Big|_{x=x_b} \le q \\ x_k = \dfrac{1}{4}\left(l + b - \dfrac{H^2}{mb}\right) & \sigma_x^{II}\Big|_{x=x_b} > q \\ \sigma_x^{II}\big|_{x=x_b} = 2K + \dfrac{mK}{H}(l-b) & \\ q = 2K\left(1 + \dfrac{H}{2b}\right) & \end{cases} \tag{2}$$

where b is the rib width, l is the width of local loading, H is the thickness of web in loading area, and K is the shearing yield strength.

$$\begin{cases} x_k = \dfrac{b}{2} & \sigma_x^{II}\Big|_{x=x_b} \le q \\ x_k = \dfrac{1}{4}(l+b) - \dfrac{\Delta H}{2m}\left(1 + \dfrac{H+\Delta H}{2b}\right) & \sigma_x^{II}\Big|_{x=x_b} > q \\ \sigma_x^{II}\big|_{x=x_b} = \dfrac{mK}{\Delta H}(l-b) & \\ q = 2K\left(1 + \dfrac{H+\Delta H}{2b}\right) & \end{cases} \tag{3}$$

where b is the rib width, l is the width of local loading, and ΔH is the thickness difference of the variable-thickness region of billet (VTRB), i.e., the thickness of layer 1, H is the thickness of layer 2, as shown in Fig. 12b.

The constrained conditions of the not loaded area for two categories of local loading state are different, and then the critical condition of switch between shearing deformation pattern and upsetting-extrusion deformation is different. The critical condition of switch was summarized in the study [53], as listed in Table 1.

The initial parameters to avoid shearing deformation in the local loading state caused by GPB are much harsher than those in the local loading state caused by GPD. However, the local loading width will increase sharply in the process with the local loading state caused by GPB, and the shearing deformation pattern will turn into an upsetting-extrusion deformation pattern quickly. In the local loading process, the extent of variation of x_k in the local loading state caused by GPB is much greater than that in the local loading state caused by GPD.

To analyze the cavity filling and second metal distribution, the analytical solution can be obtained by using Eqs. (1) and (2), but it is difficult to obtain an analytical solution by using Eq. (3) due to the nonlinear and dynamical variation of l and H. The partial least squares (PLS) regression method was introduced and used to develop the predicted model for the dynamic l in order to reduce sample size and regress multi-variables in one time [50]. The PLS regression method can model multi-response variables simultaneously with strong multi-collinear data, small sample size, and numerous predictor variables [54, 55].

Then, the H and metal inside of x_k in process with the local loading state caused by GPB can be solved by using the numerical method. The evolution of transition condition of VTRB was modeled in the study [56], and then the dynamic unrestricted portion of VTRB can be considered in Eq. (3). Based on these works, a semi-analytic fast analysis code for the multi-rib component was developed in the study [57], where the loading area is divided into finite elements according to the geometric parameters and contact condition and then the SM model Eqs. (1) to (3) are used in each element. The difference between the semi-analytic method and finite element method (FEM) is less than 10%, generally, but the consumed CPU time of the semi-analytic method is only 10^{-5} – 10^{-4} of that of FEM.

4 Friction and its influence

4.1 Friction model and friction condition

The friction model and friction condition are the key parameters in the analytical and numerical analysis of the metal forming process. The Coulomb friction model, Tresca friction model (i.e., shear friction model), and Coulomb-Tresca friction model (i.e., hybrid friction model) are widely used in bulk metal forming [58–62]. The friction models are generally expressed by Eqs. (4) to (6), respectively. In some situations, full sticking condition ($m = 1$) was adopted for the Coulomb-Tresca friction model, such as rotating compression forming [63]:

$$\tau = \mu p \tag{4}$$

$$\tau = mK \tag{5}$$

$$\tau = \begin{cases} \mu p & \mu p < mK \\ mK & \mu p \ge mK \end{cases} \tag{6}$$

where τ is the friction shear stress, μ is the Coulomb friction coefficient, p is the normal pressure, m is the Tresca friction factor, and K is the shear yield stress.

The above expressions can be used in SM, but the velocity-dependent friction models are used in the FEM due to abrupt changes of friction stress in the neutral point or region. The velocity-dependent Coulomb friction model and Tresca friction model are expressed by Eqs. (7) and (8), respectively, and combination of

Table 1 Critical geometric parameters of switch between different deformation patterns

	Shearing deformation	Upsetting-extrusion deformation
Local loading state caused by GPD	$\frac{H}{b} \geq \sqrt{m\left(\frac{l}{b}-1\right)}$	$\frac{H}{b} < \sqrt{m\left(\frac{l}{b}-1\right)}$
Local loading state caused by GPB	$\frac{\Delta H}{b} \geq \sqrt{m\left(\frac{l}{b}-1\right)} + \left(1+\frac{H}{2b}\right)^2 - \left(1+\frac{H}{2b}\right)$	$\frac{\Delta H}{b} < \sqrt{m\left(\frac{l}{b}-1\right)} + \left(1+\frac{H}{2b}\right)^2 - \left(1+\frac{H}{2b}\right)$

Eqs. (7) and (8) is used to describe the Coulomb-Tresca friction model in FEM [19, 64, 65]:

$$\tau = \mu p \left\{ \frac{2}{\pi} \arctan\left(\frac{|u_r|}{u_0} \right) \right\} \frac{u_r}{|u_r|} \tag{7}$$

$$\tau = mK \left\{ \frac{2}{\pi} \arctan\left(\frac{|u_r|}{u_0} \right) \right\} \frac{u_r}{|u_r|} \tag{8}$$

where u_r is the relative velocity and u_0 is an arbitrary constant much smaller than relative velocity.

To discuss the difference between the Coulomb friction model and Tresca friction model, the corresponding friction coefficient and friction factor should be used. Furthermore, the corresponding friction coefficient and friction factor are often used in the Coulomb-Tresca friction model.

The corresponding μ and m can be determined according to the upper limit ratio of the friction coefficient/factor. The ratio of $\mu$to m is 0.557 for the Von Mises yield criterion and 0.5 for the Tresca yield criterion. This method was used to determine the corresponding friction parameters (coefficient/factor) in the study [19, 62]. The other way to determine the corresponding friction parameters is by comparing load curves [66, 67].

By comparing calibration curves of friction tests such as the upsetting test [65] and ring compression test [68] to determine the corresponding friction parameters is also commonly adopted. The correlate relationship between the Coulomb friction coefficient and the Tresca friction factor was molded by using this method in the study [69]; the correlate relationship in cold and hot forming condition were expressed by Eqs. (9) and (10), respectively:

$$\begin{cases} \mu = km \\ k = 0.5722 - 0.44092m + 0.28119m^2, (0 < m < 0.8) \\ k = 0.39881 + 7.67533 \times 10^{-13} \exp(26.1783m), (0.7 < m < 1) \end{cases} \tag{9}$$

$$\begin{cases} \mu = km \\ k = 0.56009 - 0.36544m + 0.22712m^2, (0 < m < 0.8) \\ k = 0.41613 + 4.05049 \times 10^{-16} \exp(33.6099m), (0.7 < m < 1) \end{cases} \tag{10}$$

The friction condition evaluated by the ring compression test can be using in the hot forming analysis of the large-scale component under local loading [70]. The ring compression test of Ti-6AL-2Zr-1Mo01V alloy under 950 and 970 °C by loading speed 0.1–1.0 mm/s indicated that [70]the Tresca friction factor is 0.7 without lubricant and 0.12–0.5 with lubricant. The Coulomb friction coefficient can be determined by combining the m value and Eq. (10), and the calibration curves with the determined μ are well matched with the experimental data [71], as shown in Fig. 13.

4.2 Influence of the friction model on analysis of the local loading process

SM models described in Section 3 were based on the Tresca friction model. The SM models based on the Coulomb friction model and Coulomb-Tresca friction model were developed in the study [19] for the local loading process shown in Fig. 11f which reflects the local loading state caused by GPD. The SM model of x_k based on the Coulomb friction model can be expressed by Eq. (11), but the expression based on the Coulomb-Tresca friction model is complicated due to judgment of the friction model according to magnitude of friction shear stress:

$$\begin{cases} x_k = \dfrac{b}{2} & \sigma_x^{\mathrm{II}}\Big|_{x=x_b} \leq q \\ x_k = \dfrac{1}{4}\left(l + b - \dfrac{H}{\mu} \ln\left(1 + \dfrac{H}{4b} \right) \right) & \sigma_x^{\mathrm{II}}\Big|_{x=x_b} > q \\ \sigma_x^{\mathrm{II}}\big|_{x=x_b} = 4Ke^{\frac{\mu}{H}(l-b)} - 2K \\ q = 2K\left(1 + \dfrac{H}{2b} \right) \end{cases} \tag{11}$$

According to stress at interface, the scope of the Coulomb-Tresca friction model at interface is shown in Fig. 14 [19], where the critical values x_m^{II} and x_m^{III} can be solved according to the SM model with respect to stress based on different friction models in regions II and III, and can be expressed by Eqs. (12) and (13), respectively:

$$x_m^{\mathrm{II}} = x_l - \frac{H}{2\mu} \ln\left(\frac{m}{4\mu} \right) \tag{12}$$

$$x_m^{\mathrm{III}} = x_b + \frac{H}{2\mu} \ln\left(\frac{mb}{\mu(4b+H)} \right) \tag{13}$$

The ratio of $\mu$to m presented in Eqs. (9) and (10) is greater than 0.4 according to research in the study [69], which is also supported by other publications [66–68]. If $\mu/m > 0.25$, the

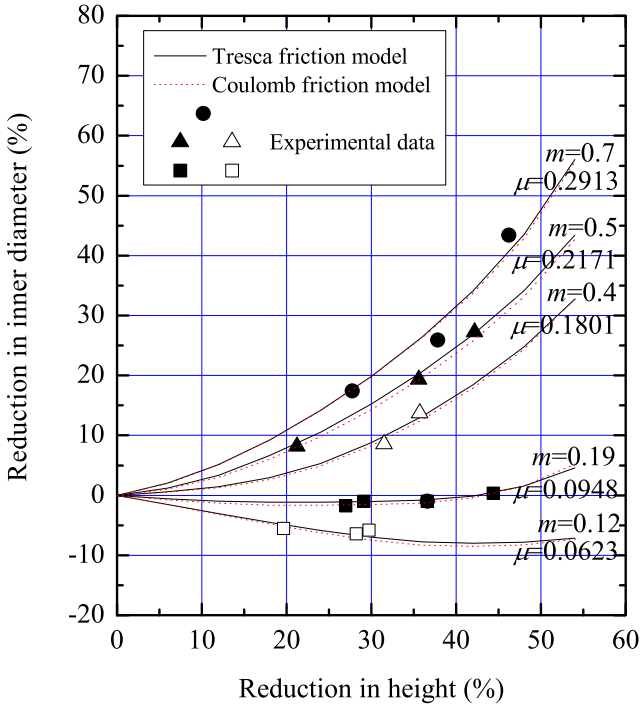

Fig. 13 Calibration curves under different friction models and experimental data [71]

real solution to Eqs. (12) and (13) are $x_m^{II} > x_l$ and $x_m^{III} < x_b$, respectively, and thus the Coulomb-Tresca friction model degenerates into the Tresca friction model in the SM model [19]. And the FEM results also indicated that the predicted load-stroke curve and the predicted distributions of stress and strain adopted Coulomb-Tresca model are similar to those adopted Tresca friction model, but are different from those adopted Coulomb friction model. Figure 15 illustrates the distributions of effective stress in the local loading state caused by GPD.

It can be found from Fig. 15 that the predicted rib height adopted Coulomb friction model is higher than that adopted Tresca friction model. The reasons are that [19] the predicated range of geometric parameters to avoid shearing deformation adopted Coulomb friction model is larger than that adopted Tresca friction model, and the predicated x_k adopted Coulomb friction model is larger than that adopted Tresca friction model, as shown in Fig. 16.

Deformation characteristics in the local loading state caused by GPB are similar to that caused by GPD although there are different constrained boundaries. Thus, influences of friction models on predicted results are similar. However, the local loading state caused by GPB will turn into the whole loading state. The difference of predicted results among different friction models were investigated in the study [71]. And the results indicated that the Coulomb-Tresca friction model also degenerates into the Tresca friction model, as shown in Fig. 17, and predicted rib height adopted Coulomb friction model is also higher than that adopted Tresca friction model at the local loading stage.

Compared with the experimental data of T-shaped component local loading, the predicted value by the Tresca friction model is much closer to experimental load [19] and experimental rib height [19, 71]. Thus, the Tresca friction model may be suitable for analysis of the local loading process.

4.3 Influence of friction condition on the local loading process

The variation of friction condition will lead to change in load, deformation pattern, and metal flow. The deformation pattern and metal flow will influence the cavity filling and forming defects.

Generally, the direct influence of friction on load is less than 5%. However, the friction influences the constraint condition and stress state in the forming process, especially for the complex component and the local loading forming process. For the second local loading step of the component shown in Fig. 7b, discrepancy between the predicted load by FEM with $m = 0.3$ and experimental data is greater than 30% [71], where the Tresca friction factor 0.3 is a recommended upper limit for hot forming of titanium alloy with glass lubricants [58]. However, the glass lubricants used in the experiment contains some graphite, and the magnitude of friction is about 0.5 for the experiment conditions. The relative error of load is less than 15% when the $m = 0.5$ was adopted in FEM [72].

It can be found from Table 1 that magnitude of friction plays an important role on the critical condition of switch between shearing deformation pattern and upsetting-extrusion deformation. With the increase of friction, the geometrical parameters to avoid shearing deformation in the local loading state will be expanded [53], as shown in Fig. 18.

The shear deformation will result in under-filling [53] and superabundant metal flowing outward will do harm to the formation of neighbor rib [49]. Increasing magnitude of friction will reduce shear deformation. Furthermore, the x_k in the upsetting-extrusion deformation pattern increases with the

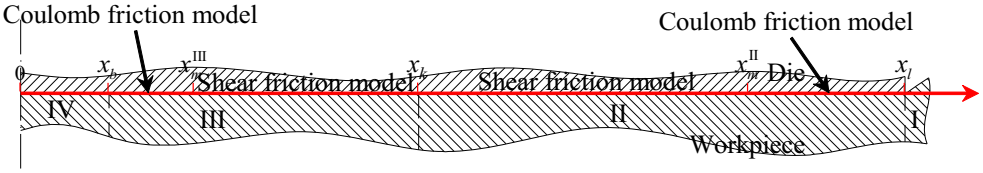

Fig. 14 Coulomb-Tresca friction model at interface in local loading state

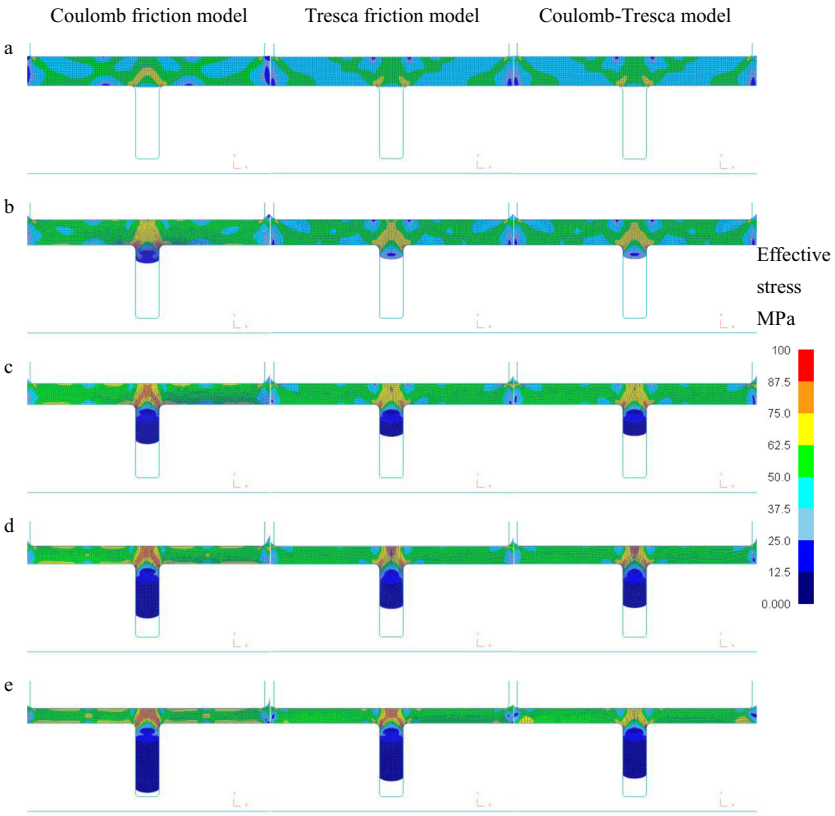

Fig. 15 Distributions of effective stress at chosen stages in the process shown in Fig. 11f [19], stroke is **a** 0.25 mm, **b** 1.50 mm, **c** 3.00 mm, **d** 4.00 mm, and **e** 5.00 mm

increase of friction according to Eqs. (2) and (3). To improve cavity filling by increasing friction was also proven by the experiment and FEM, and the increase in x_k with increasing friction was also proven by FEM [53]. Quantitative calculation of the volume of metal indicated that [73] the transverse-flowing metal will reduce with increasing friction.

The metal flowing outward, i.e., the transverse-flowing metal, flows into the not loaded area, and will result in folding in web and cavum in the rib (as shown in Fig. 19a) [74], and folding in the formed rib [49], and the piercing rib at the end of the formed rib [53]. The metal flowing into the not loaded area will be reduced as friction increases, and then the length of folding and depth of cavum will decrease (as shown in Fig. 19b) [74], and thus some defects will be suppressed by increasing friction.

Metal flow can be controlled by adjusting and controlling friction in the proper range of friction, and then cavity filling can be improved and forming defects can be suppressed.

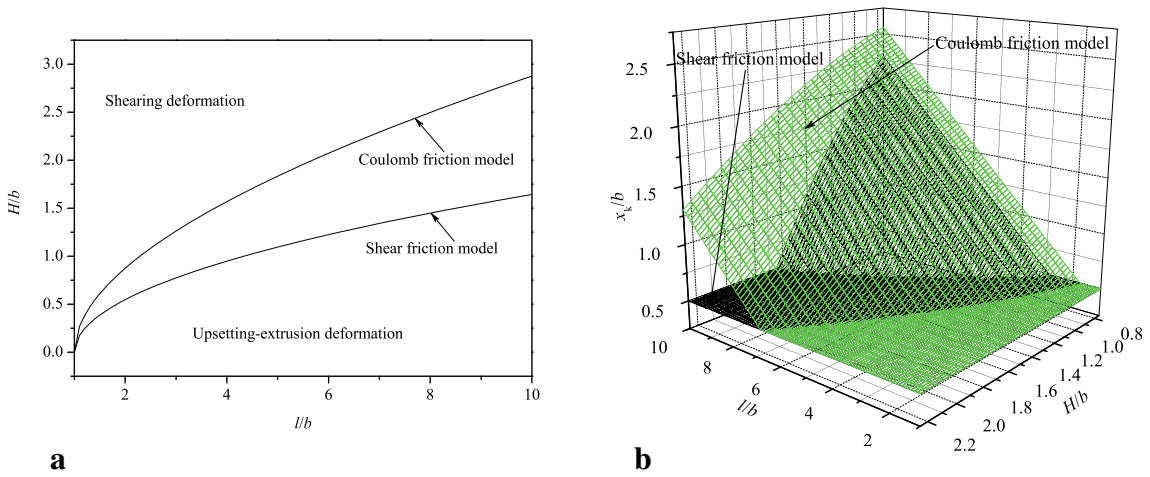

Fig. 16 Deformation characteristics under different friction models [19]: **a** deformation pattern and **b** neutral layer

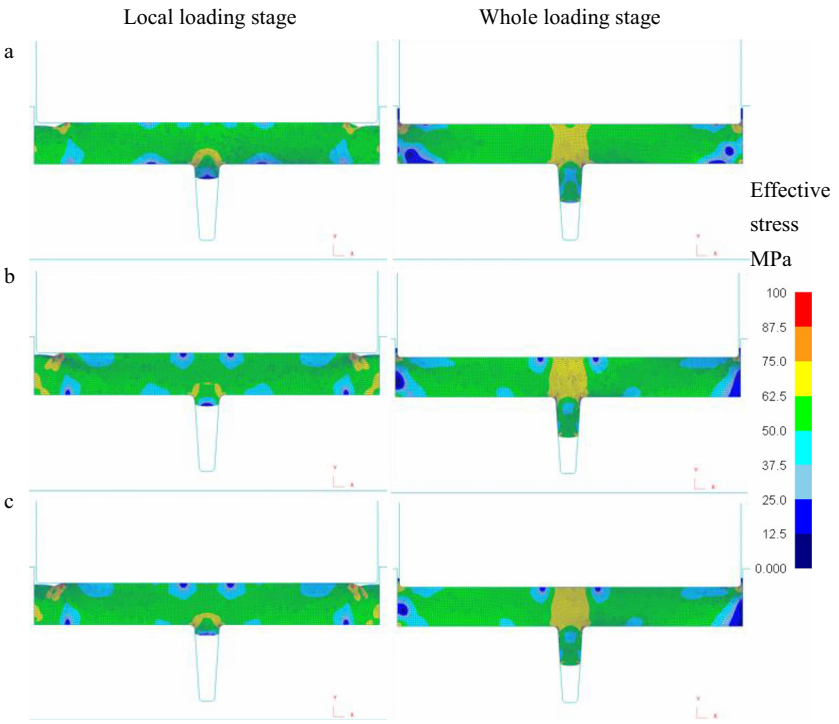

Fig. 17 Distributions of effective stress in different loading states in the process shown in Fig. 11g [71]: **a** Coulomb friction model, **b** Tresca friction model, and **c** Coulomb-Tresca friction model

Figure 20 illustrates some FEM examples for adjusting and controlling friction in the local area to improve cavity filling and suppress defects. The friction condition can be controlled by lubricant or loading speed [70], or preparing the surface of the die [75]. Combining control of friction with other parameters, especially the shape of billet, will lead to a better result.

5 Forming defects and process control

5.1 Typical forming defect

The forming defects such as under-filling, folding, problem of flow lines in the whole forging [76] also present in the local loading [31, 36, 49, 53, 77]. The forming defects in the local loading process are mainly caused by the metal flowing from the loading area into the not loaded area. A rib-shift (Fig. 21a) is caused by this metal flow [77, 78] near the die partitioning boundary. As a result of overabundant rib-shift, folding (Fig. 21b) occur [77]. The folding defect also occur in the variable-thickness region of the billet in the third local loading state due to second metal distribution, as shown in Fig. 21c [50, 79]. The folding may be avoided by preform design and parameter control, which will be discussed in the following sections.

The burr on the partitioning boundary occurs due to tolerance clearance between sub-dies [77, 78, 81], as shown in Fig. 21d, e. Artificial gap between sub-dies can accommodate

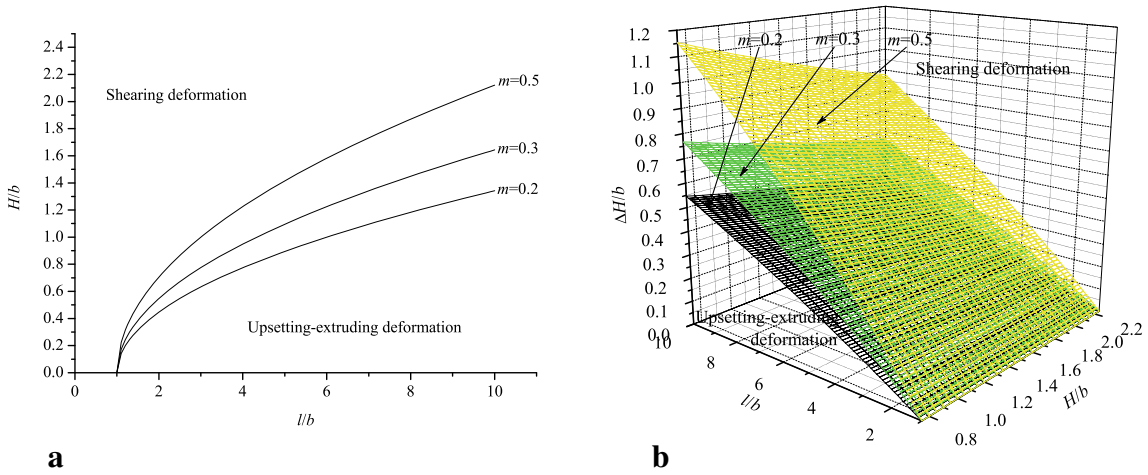

Fig. 18 Deformation pattern under different friction conditions [53], local loading patterns caused by **a** GPD and **b** GPB

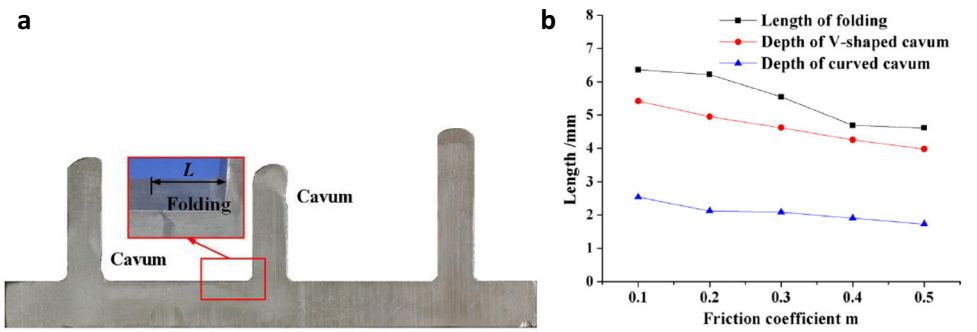

Fig. 19 Defects in first local loading zone in second local loading step [74]: **a** sketch of defects and **b** influence of friction

the transverse-flowing metal to reduce burr, but a bulge (Fig. 21f) may occur [80], and a haunch-up (Fig. 21g) may occur [51] when the gap increases even further. Under partition at the rib, the rib cavity can accommodate the transverse-flowing metal and burr defect may be avoided [78, 81]; however, the burr also occurs after complete die filling [77], as shown in Fig. 21e. The burr (Fig. 21d) is longer and difficult to clean under partition at web, but the burr on the partitioning boundary at the rib is small. The phenomenon that much redundant metal flows in one direction is prone to appearing near the die partitioning boundary. And thus the defects about metal flow lines, such as flow lines disturbance and fibber breaking as shown in Fig. 21h, i, are prone to occurrence [77].

5.2 Deformation characteristic of the transitional deformation zone

Three representative deformation zones are presented in the local loading process, such as the plastic yield deformation zone, non-yield deformation zone, and transitional deformation zone between the first two zones. The transitional deformation zone is a part of the not loaded area, and it is defined as the region near the plastic yield deformation zone but without restriction of the die [51, 78, 82, 83], as shown in Fig. 22. However, the transitional deformation zone is a physical reality, and it coordinates the severe plastic yield state and non-yield state; the coordinating range is prone to being wider than the traditional transitional deformation zone, especially the transitional deformation zone in Fig. 22a.

Thus, the transitional deformation zone is a coordination zone of deformation from plastic yield deformation to non-yield deformation. Its range is larger than the defined zone in Fig. 22, and depends on the material, loading condition, die geometry, billet geometry, and so on [18, 79]. Excepting the transitional deformation zone near the die partitioning boundary, which was focused strongly, the other main is the transitional deformation zone near the VTRB. In essence, the forming defects are the coordination product of unequal deformation between the plastic yield deformation zone and non-yield deformation zone.

5.2.1 Transitional deformation zone near variable-thickness region of billet

The folding is the main defect in VTRB, and it is developed from V-shaped cavum such as accumbent V-shaped cavum, upright V-shaped cavum, and hand-stand V-shaped cavum

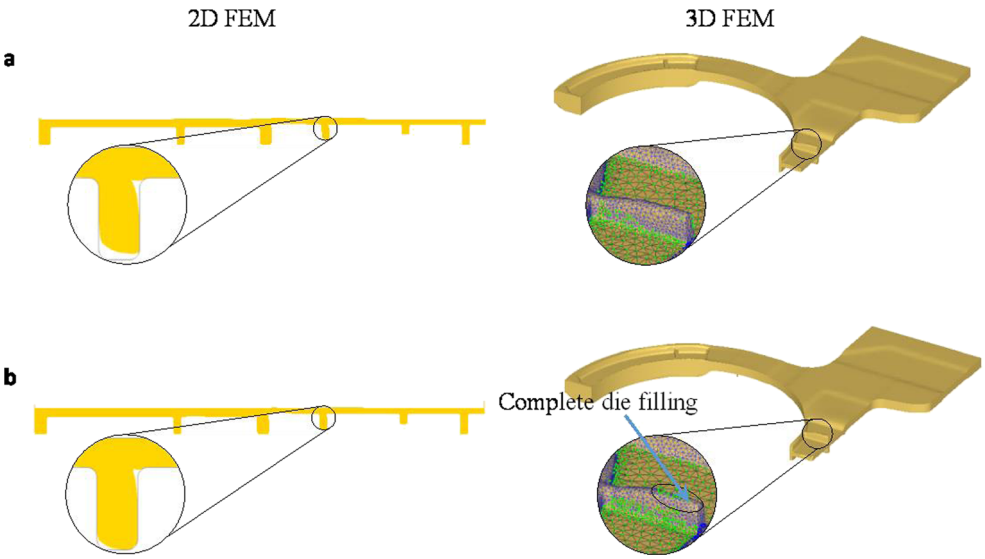

Fig. 20 Forming quality under different friction [53]: **a** $m = 0.3$, **b** $m = 0.3$, and $m = 0.5$

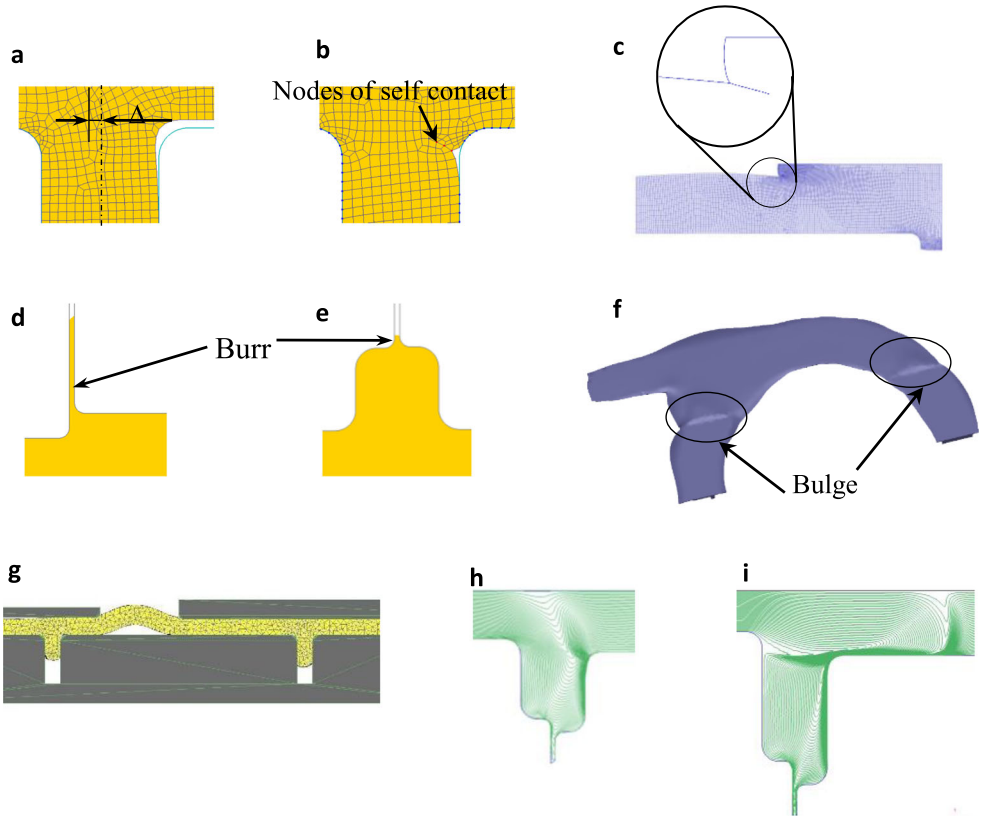

Fig. 21 Possible forming defects in local loading process: **a** rib-shift [77], **b** folding in formed rib [77], **c** folding in VTRB [79], **d** burr on partitioning boundary at web [77], **e** burr on partitioning boundary at rib [77], **f** bulge in gap between sub-dies [80], **g** haunch-up in gap between sub-dies [51], **h** flow lines disturbance [77], and **i** fibber breaking [77]

[79], as shown in Fig. 23. The transverse flow of metal is caused by local loading. And the upper and lower flowing velocities of transverse-flowing metal are different due to the restriction of the die and not loaded area, and then some metal builds up and warps to form V-shaped cavum [18, 79].

The V-shaped cavum may be planished or result in defect, which is determined by transition pattern, transition condition, and located position of VTRB. Because of the simple pattern and wide transition condition, the beveling transition pattern should be selected prior for VTRB, especially for the large thickness of VTRB or VTRB near the rib cavity or die partitioning boundary [56, 79]. The transition condition $R_b$under the beveling transition pattern is defined by Eq. (14) [79]:

$$R_b = \frac{\Delta l}{\Delta H} \tag{14}$$

where ΔH is the thickness difference of VTRB and $\Delta l$is the length of beveling.

The VTRB should avoid being set near the rib cavity or die partitioning boundary, and the large R_b should be adopted if VTRB is set at these positions [79]. For example, R_b=10 was adopted for a VTRB that near rib cavity in the study [79], and a large transition condition also was adopted for VTRB due to locating near cavity [49], and then the folding was not observed according to FEM results. The located position and transition condition were adopted according to the recommendations above in the preform design of a large-size bulkhead of titanium alloy [84, 85].

5.2.2 Transitional deformation zone near the die partitioning boundary

The transverse metal flow with opposite direction for different local loading step is a typical characteristic in the transitional deformation zone near the die partitioning boundary. Various defects, such as rib-shift, folding, and flow lines defects, may

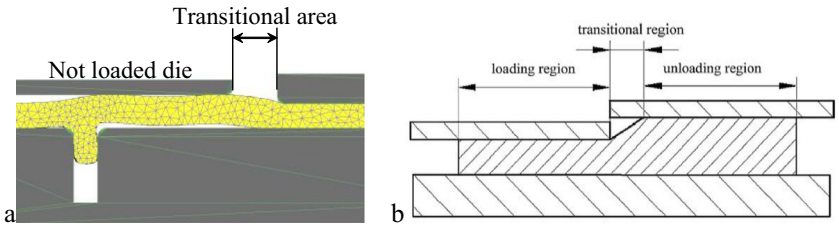

Fig. 22 Definition of traditional transitional deformation zone: **a** definition in [51] and **b** definition in [82, 83]

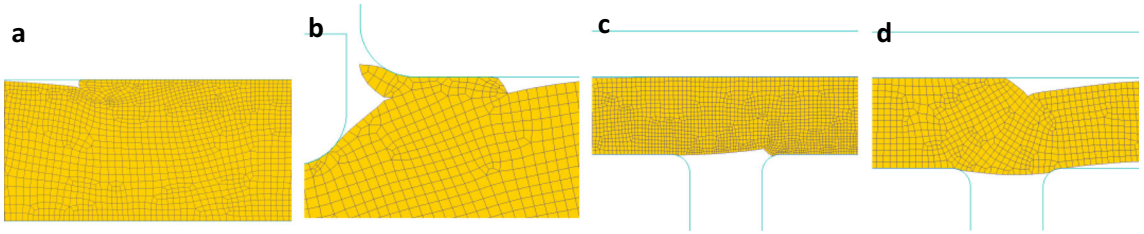

Fig. 23 V-shaped cavum in VTRB: **a** VTRB at web [79], **b** VTRB near die partitioning boundary [79], **c** VTRB on the side near rib cavity [18], and **d** VTRB on the opposite side near rib cavity [18]

occur in the transitional deformation zone around the die partitioning boundary due to the transverse flow. However, the influence of the transverse metal flow is short [78, 86], the influence mainly presents in the region from the die partitioning boundary to the first rib in the not loaded area [77]. And the geometric parameters play an important role on the forming defects [77, 87].

The die partitioning boundary at the rib is a better partitioning pattern. In the first local loading step, the cavity of the partitioning rib is filled after the constraint clearance between the partitioning boundary and the first rib cavity in the not loaded area is completely filled [77]. About 40–80% of transverse-flowing metal (i.e., the metal flowing from the loading area into the not loaded area) fills the cavity of the partitioning rib in the second local loading step [87]. And the ratio (y) of transverse-flowing metal flowing into the cavity was modeled by the PLS regression method, which are expressed as follows [87]:

$$y = 70.3184 - 12.5083x_1 - 1.8182x_2 + 9.8023x_5 \tag{15}$$

where x_i is the geometric parameters about constraint clearance, distance between ribs, rib width, and rib height.

The transverse flow leads to some problem. Thus, based on DEFORM-2D, a quantitative-calculation subroutine of volume for flowing metal was developed in the study [73]. The results indicated that the metal in the not loaded area will increase notably although the final volume is almost equal to the initial volume, as shown in Fig. 24.

The final volume in the first or second local loading area is almost equal to the initial volume. However, the lost volume in the first local loading area is recovered after cavity filling, which is needless. Thus, the forming defects often occur in the first local loading area during the second local loading step [73, 74]. Especially local loading way on ordinary single-action hydraulic press shown in Fig. 10 being adopted, root of partitioning rib is prone to being extruded (region D in Fig. 25) to form defect at the late forming stage.

The local loading way on the double-action press shown in Fig. 9 can provide a better forming quality due to the smaller transverse metal flow [88]. The reason is that the double-action hydraulic press can provide a smaller constraint clearance on the not loaded area, but the constraint clearance is from the thickness of the spacer block to zero during the second loading step by using the ordinary single-action hydraulic press. Thus, reducing thickness of the spacer block could eliminate folding [73, 74].

The geometric parameters of dies and billet play an important role on the forming defects such as folding. In order to control the forming defect in the transitional deformation zone, it is necessary to predict the magnitude of folding quickly and model the relationship between folding and geometric parameters. A folding index ϕ expressed by Eq. (16) has been developed according to the deformation characteristic and geometrical characteristic in the transitional deformation zone during the local loading forming process [89]:

$$\phi = \int_{t_0}^{t_{fold}} \left(\frac{1}{\int_{\partial\Omega_{foldzone}} ds} \frac{s_{ref}}{s_{ave}} \int_{\partial\Omega_{foldzone}} \dot{\bar{\varepsilon}} ds \right) dt \tag{16}$$

where t_0 is the initial time of the second loading step; t_{fold} is the time when development of folding finishes; $\partial\Omega_{foldzone}$ is the free surface in folding zone; s_{ref} is the reference area; $s_{ave} = \left(1/nbelt'\right)\sum_1^{nbelt'} s_i$, where $nbelt'$ is the total number of free surface elements in folding zone; and s_i is the area of element.

Then, relationship between folding index ϕ and geometric parameters such as distance between ribs, rib width, thickness

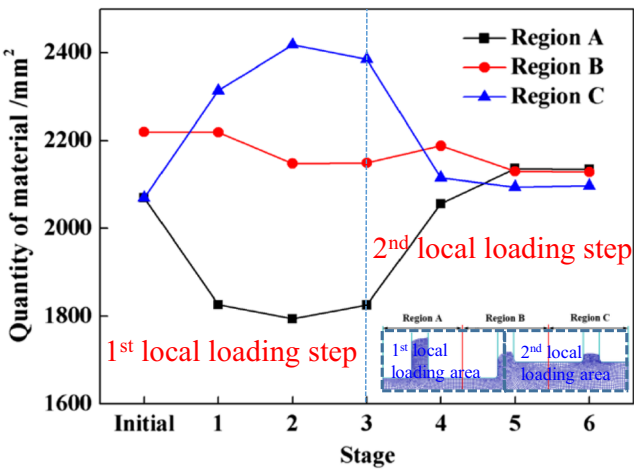

Fig. 24 Volume of metal in different areas during local loading forming process [73]

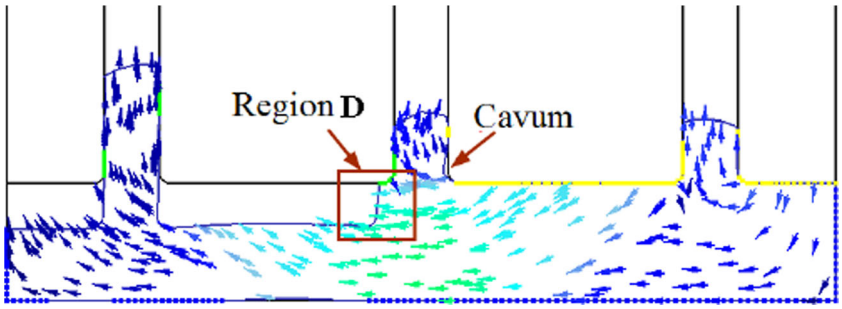

Fig. 25 Velocity distribution of metal flow during second local loading step [74]

of billet, and thickness of the spacer block has been modeled by the response surface method (RSM) [89], Kriging metamodel [90], and back-propagation neural network [91]. Figure 26a illustrates the relationship between value of ϕ and length of folding, so the critical C_1 and C_2 can be chosen to judging folding [89], as shown in Fig. 26b. In practice, the geometric parameters making ϕ less than C_1 should be adopted.

5.3 Influence of forming parameters on the local loading process

The reduction during loading pass is determined by the number of loading pass. Loading sequence during loading pass has an influence on constraint state in the loading area, especially for some special loading way and shape of the workpiece. The research in the study [46] indicated that influence of loading pass on the forming force is less than the influence of the loading sequence on the forming force in the local loading process of aluminum alloy forging shown in Fig. 8c, and the loading sequence has a notable influence on cavity filling.

Area of sub-die has some influences on other aspects except loading load. Increasing the area of the middle sub-die and reducing the area of the side sub-dies may increase the offset force [86]. Setting an appropriate overlapping loading area between two local loading areas can eliminate the bulge and reduce rib-shift [80]. However, it is difficult in the industrial practice.

Some details of geometric parameters, such as draft angle (γ) and the fillet radius (r), between a rib and web were not considered in the mentions in the above sections such as Sections 3, 4, and 5.2. The aerospace and aircraft components such as rib-web component are with a small even zero draft angle [92]. However, the fillet radius could be considered. An analytical SM model considering $\gamma$and r was developed in the study [93] to describe the local loading process shown in Fig. 11f. The SM analysis indicated that the fillet radius has an influence on cavity filling, but draft angle has little influence on cavity filling, as shown in Fig. 27. Generally, the error between two SM models is less than 10% in $r/b = 0.25$–0.75.

Conversely, the draft angle has an influence on final load, but fillet radius has little influence on final load although low load with large fillet radius at initial stage [93]. Considering draft angle 1.5°, the error of the forming load between 3D-FEM and the experiment during the second local loading step of the component shown in Fig. 7b dropped from 15 to 10% [93].

There are two kinds of strain concentration presenting in the transitional deformation zone around the die partitioning boundary, and one is caused by symmetric filling and one is caused by transverse metal flow with opposite direction during multi-local loading [94]. The relationship between the inhomogeneity index and geometric parameters such as $\gamma$and r was modeled by using RSM, and optimization results indicated that draft angle of cavity of the partitioning rib should be larger than others [94]. The forming defects in the transitional deformation zone around the die partitioning

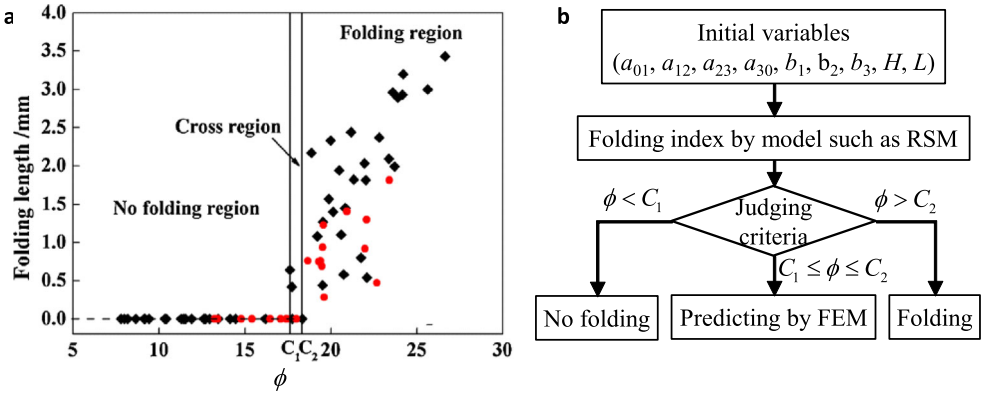

Fig. 26 Judging criteria of folding [89]: **a** ϕ vs. length of folding and **b** prediction of folding

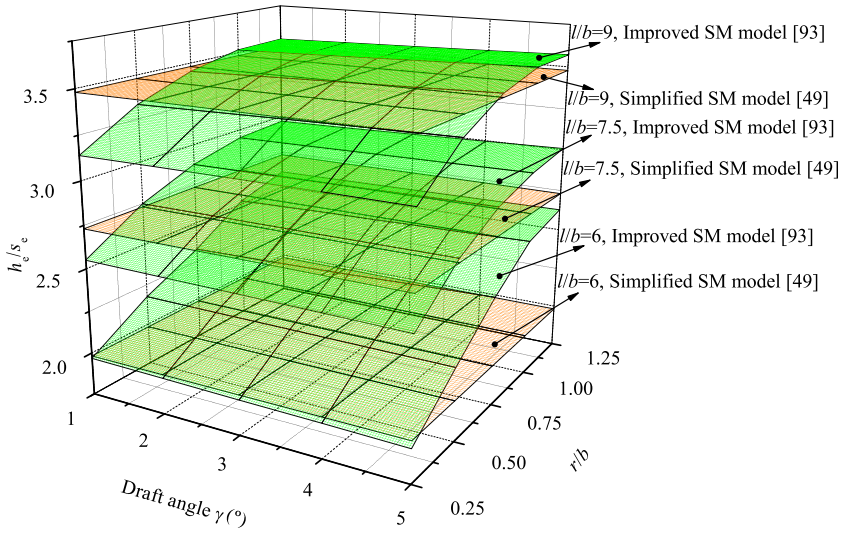

Fig. 27 Predicted rib heights after local loading by different SM model [93]

boundary occur in the first local loading area during the second local loading step. 2D-FE results indicated that [95] only geometric parameters such as $\gamma$and r of cavities of the partitioning rib and rib in the first local loading area present an influence, and the limit stroke (L_{max}) of the die can be extended with increasing the fillet radius.

5.4 Process control of local loading technology

The proper local loading way can improve the forming itself. For instance, the cavity filling of peripheral rib was improved by peripheral local loading [30, 36], and the folding and flow lines disturbance at the root of the rib were avoided by local loading [37]. More commonly, combing local loading with preform design can be used to control the forming process and to improve the forming quality.

The initial metal distribution can be carried out by simple UTB with short time and low cost, so the UTB is often used in industrial practices. According to FEM and physical modeling experimental results, a UTB was designed to distribute enough metal for four ear-cavities of magnesium alloy upper housing forging, and then cavity filling was improved with local loading way [33], and the folding at ear was also avoided [32]. The thicknesses of two parts of the billet were determined according to volume of the easy forming region and difficult forming region [96], respectively, and there are some improvements in cavity filling. Considering the local loading characteristic, a UTB of a large-size titanium ally bulkhead was designed by the analytical and 3D-FEM hybrid method [84], where Eqs. (1)–(3) were adopted.

Control of the forming process and elimination of forming defect also can be done by choosing a suitable forming parameter according to the principle of forming. The optimization methods also can be introduced into the process control when the forming process or forming parameter is simple. Based on the sample data provided by FEM, the relationship between single-object (grain size uniformity or filling capacity) and forming parameters was independently modeled by RSM, and then the objective function of forming quality including two objects was modeled based on linear weighting method [45]. The suitable temperature of the billet, speed of press, number of loading pass, and draft angle were determined according to the objective function. By using RSM and sample data provided by 3D-FEM, the UTB for the transitional deformation zone near the die partitioning boundary was designed by taking deformation homogeneity [97] and improvement of filling and folding [98] as optimization objective, respectively.

In general, the process control is carried out by controlling processing parameters and geometrical parameters. Isothermal forming with low loading speed is often adopted to manufacture a complicated component made by hard-to-deform material. Thus, the ranges of adjusting temperature and loading speed are narrow, which are determined by material parameters. Then, the process control of local loading technology is mostly carried out by adjusting die partition, shape of billet, friction condition, etc.

The large-size component has a complicated structure such as high ribs and thin web, and an extreme size feature such as 5 mm in fillet radius and more than 1000 mm in length and width [79]. Thus, number of parameters or design variables for increases greatly, and choosing design variables and modeling objective function are difficult, and determination of dynamical boundary condition in backward simulation is also difficult, and the numerical simulation of the through forming process by 3D-FEM takes long CPU time [84].

The reasonable range of geometrical and processing parameters, which is close to the optimal results, can be quickly determined by an analytical method such as SM. Then, 3D-FEM is used to search for the optimal results, where the

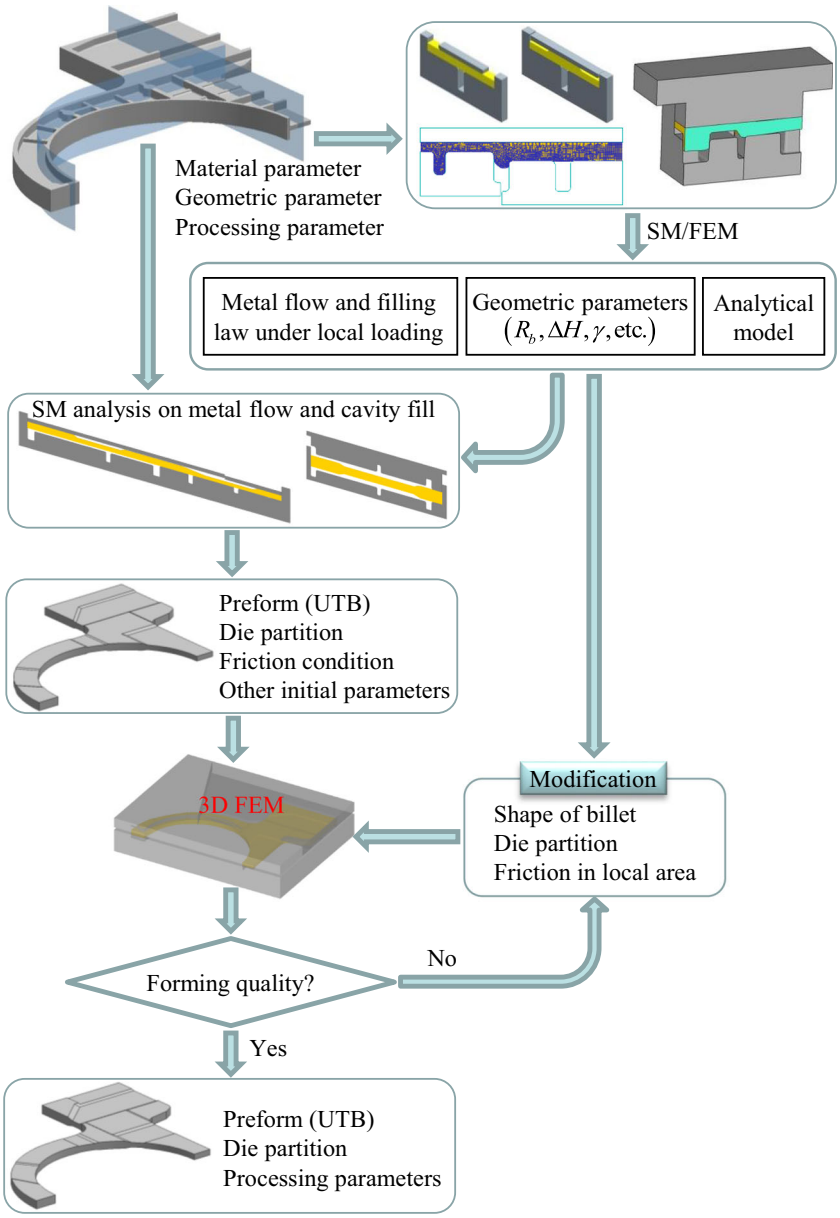

Fig. 28 Method of process optimization of local loading process for large-size component

number of numerical simulation can be reduced. This analytical and 3D-FEM hybrid method may be an appropriate approach to optimize the local loading process of a large-size complicated component. A UTB was designed by using this method [84], where modification based on 3D-FEM results is only twice. The hybrid method can be summarized in Fig. 28.

6 Conclusions

The intermittent local loading technology can reduce forging load, control metal flow, and expand the size of available formed component. It is suitable to manufacture an irregular integral component with large-size. Especially, local loading combing with isothermal forging provides a feasible approach to manufacture a large-size complicated component of hard-to-deform material with less force and lower cost.

From local loading by simple punch to local loading by bolster plate and to local loading by partial die, the flexibility of the process is diminishing progressively, and the forming process is simplified progressively, but the available formed component is more and more complex progressively. The microstructure and mechanical properties of the component manufactured by local loading meet the design requirements. For instance, the grain sizes of Cu lid formed by LLbSP is much less than that set by the company, which meets the requirements [30]; mechanical properties of titanium alloy forging formed by LLbBP are slightly more than design requirements [37]; mechanical properties of titanium alloy headbulk formed by LLbPD are close to whole near

βforging, and some mechanical properties are superior to whole α+βforging [25, 99].

Acknowledgements This work is for the memory of Prof. He Yang. The work was supported in part by the National Natural Science Foundation of China (Grant No. 51675415) and the fund of the State Key Laboratory of Solidification Processing in NWPU (SKLSP201623).

References

1. Kleinera M, Geigerb M, Klaus A (2003) Manufacturing of lightweight components by metal forming. CIRP Ann Manuf Technol 52(2):521–542
2. Yang H, Zhan M, Liu YL, Xian FJ, Sun ZC, Lin Y, Zhang XG (2004) Some advanced plastic processing technologies and their numerical simulation. J Mater Process Technol 151:63–69
3. Moiseyev VN (2006) Titanium alloys: Russian aircraft and aerospace applications. Taylor & Francis Group, Boca Raton
4. Yang H, Fan XG, Sun ZC, Guo LG, Zhan M (2011) Recent development in plastic forming technology of titanium alloys. Sci China Tech Sci 54(2):490–501
5. Zhang DW, Yang H (2012) Isothermal local loading forming technology of large-scale integral titanium alloy bulkhead. Forg Metalform 21:32–38 (in Chinese)
6. Huang X, Wang B, Zhou J, Ji H, Mu Y, Li J (2017) Comparative study of warm and hot cross-wedge rolling: numerical simulation and experimental trial. Int J Adv Manuf Technol 92:3541–3551
7. Zhuang W, Hua L, Wang X, Liu Y, Han X, Dong L (2015) Numerical and experimental investigation of roll-forging of automotive front axle beam. Int J Adv Manuf Technol 79:1761–1777
8. Zhu S, Yang H, Guo L, Hu L, Chen X (2014) Research on the effects of coordinate deformation on radial-axial ring rolling process by FE simulation based on in-process control. Int J Adv Manuf Technol 72:57–68
9. Han X, Hua L (2012) Investigation on contact parameters in cold rotary forging using 3D FE method. Int J Adv Manuf Technol 62: 1087–1106
10. Zhan M, Guo J, Fu MW, Li R, Gao PF, Long H, Ma F (2018) Formation mechanism and control of flaring in forward tube spinning. Int J Adv Manuf Technol 94:59–72
11. Zhang DW, Zhao SD, Ou HA (2016) Analysis of motion between rolling die and workpiece in thread rolling process with round dies. Mech Mach Theory 105:471–494
12. Yang X, Dong X, Wu Y (2017) An upper bond solution of forging load in cold radial forging process of rectangular cross-section billet. Int J Adv Manuf Technol 92:2765–2776
13. Zhang Q, Jin K, Mu D, Zhang Y, Li Y (2015) Energy-controlled rotary swaging process for tube workpiece. Int J Adv Manuf Technol 80:2015–2016
14. He X (2011) Effects of manipulator compliant movements on the quality of free forging based on FEM simulation. Int J Adv Manuf Technol 56:905–913
15. Bračun D, Škulj G, Kadiš M (2017) Spectral selective and difference imaging laser triangulation measurement system for on line measurement of large hot workpieces in precision open die forging. Int J Adv Manuf Technol 90:917–926
16. Kopp R, Schmitz A (1996) Plastic working in Germany and related environmental issues. J Mater Process Technol 59(3):186–198
17. Zhang DW, Zhao SD, Ou HA ((2016)) Motion characteristic between die and workpiece in spline rolling process with round dies. Adv Mech Eng 8(7):1–12
18. Zhang DW (2012) Forming regulation and preform design of large-scale complex titanium alloy component in isothermal local loading process. PhD Dissertation, Northwestern Polytechnical University. (in Chinese)
19. Zhang DW, Yang H (2015) Analytical and numerical analyses of local loading forming process of T-shape component by using Coulomb, shear and hybrid friction models. Tribol Int 92:259–271
20. Groche P, Fristsche D, Tekkaya EA, Allwood JM, Hirt G, Neugebauer R (2007) Incremental bulk metal forming. CIRP Ann Manuf Technol 56(2):635–656
21. Xia Q, Xiao G, Long H, Cheng X, Sheng X (2014) A review of process advancement of novel metal spinning. Int J Mach Tool Manuf 85:100–121
22. Zhi Y, Wang X, Wang S, Liu X (2018) A review on the rolling technology of shape flat products. Int J Adv Manuf Technol 94: 4507–4518
23. Yang H, Wu C, Li HW, Fan XG, Zhang DW, Ji Z (2011) Review on development of key technologies in plastic forming of titanium alloy. Mater China 30(6):6–13
24. Yang H, Fan XG, Sun ZC, Guo LG, Zhan M (2011) Some advances in local loading precision forming of large scale integral complex components of titanium alloys. Mater Res Innov 15(s1):S493–S498
25. Yang H, Li HW, Fan XG, Sun ZC, Zhang DW, Guo LG, Li H, Zhan M (2011) Technologies for advanced forming of large-scale complex-structure titanium components. In: Hirt G, Tekkaya AE (eds) Proceedings of the 10th International Conference on Technology of Plasticity (ICTP2011). Verlag Stahleisen Gmbh, Dusseldorf, pp 115–120
26. Altan T, et al (1982) Modern forging: equipment, materials and process, Lu S, translated, Defence Industrial Press, Beijing (in Chinese)
27. Welschof K, Kopp R (1987) Incremental forging—a flexible forming technology which improves energy and material efficiency. Aluminium 63(2):168–172 (in German)
28. Sturm JC, Welschof K, Binding J, Janssen W, Mahlke M, Sprangers W (1987) Methods of saving energy and materials in the manufacture of integrated aircraft structural components. Aluminium 63(11):1157–1162 (in German)
29. Lee YH, Kopp R (2001) Application of fuzzy control for a hydraulic forging machine. Fuzzy Set System 188(1):99–108
30. Ssemakula H, Ståhlerg U, Öberg K (2006) Close-die forging of large Cu-lids by a method of low force requirement. J Mater Process Technol 178:119–127
31. Hao NH, Xue KM, Lü Y (1998) Numerical simulation on forming process of ear portion of upper case. Trans Nonferrous Met Soc China 8(4):602–605
32. Lü Y, Shan DB, Xue KM, Wang Z, Xu FC, Kong XY, Zhao YZ, Hao NH (2000) Research and application on isothermal precision forging process of large and complex forging [J]. Machinist Metal Form (2):15–16 (in Chinese)
33. Shan DB, Hao NH, Lu Y (2004) Research on isothermal precision forging processes of a magnesium-alloy upper housing. In: Ghosh S, Castro JC, Lee JK (eds) AIP Conference Proceedings, vol 712. American Institute of Physics, Melville, New York, pp 636–641
34. Yang P, Shan DB, Gao SS, Xu WC, Lv Y (2006) Research on isothermal precision technology of rib-web forging parts. Forg Stamp Technol 31(3):55–58 (in Chinese)
35. Si CH, Shan DB, Lu Y (2006) Research on the key technology of near net forming of aluminum alloy hatch. Mater Sci Technol 14(3): 236–239, 243 (in Chinese)
36. Shan DB, Xu WC, Si CH, Lu Y (2007) Research on local loading method for an aluminium-alloy hatch with cross ribs and thin webs. J Mater Process Technol 187–188:480–485

37. Li L, Liu XL (2010) Research on hot-die forging technology for titanium alloy diaphragm forging. Forg Stamp Technol 35(6):11–13 (in Chinese)
38. Martin WA (1972) Heavy press forging apparatus and method. United States Patent, US3638471
39. Martin WA (1978) Forging press and method. United States Patent, US4096730
40. Delgado HE, Howson TE (1998) Closed-die forging process and rotationally incremental forging press. European Patent, EP0846505A2
41. Ren YL, Nie SM (2000) Research on new forging method of large integral container head. Heavy Mach 5:20–22 (in Chinese)
42. Zhou XH, Guo HZ (2003) Die design for super-large rotating disc forging. Forg Stamp Technol 28(5):65–68 (in Chinese)
43. Fan SQ, Zhao SD, Han XL, Xu F, Zhang Q (2012) Numerical simulation and experiment of new forming process of shroud disk of impeller. Forg Metalform 21:40–47 (in Chinese)
44. Sarkisian JM, Palitsch JR, Zecco JJ (1999) Stepped, segmented, closed-die forging. United States Patent, US5950481
45. Wang MH, Ma PC, Zhou JF, Wu DX, Zeng QH (2017) Control of local loading forming quality for aluminum alloy heavy forging based on RSM. J Cent South Univ (Sci Technol) 48(5):1155–1161 (in Chinese)
46. Zheng SJ, Zhou J, Li J, Wu DX, Zhou JF, Zhao TS (2017) Quality control on local loading of a large air aluminum-alloy forging. Forg Stamp Technol 42(9):1–5 (in Chinese)
47. Zhang DW, Li HJ, Dong P, Zhao SD (2017) A hydraulic system of local loading hydraulic press. China Patent, 201711270024.9. (in Chinese)
48. Zhang DW, Yang H (2015) Loading state in local loading forming process of large sized complicated rib-web component. Aircr Eng Aerosp Technol 87(3):206–217
49. Zhang DW, Yang H, Sun ZC (2010) Analysis of local loading forming for titanium-alloy T-shaped components using slab method. J Mater Process Technol 210:258–266
50. Zhang DW, Yang H (2013) Metal flow characteristics of local loading forming process for rib-web component with unequal-thickness billet. Int J Adv Manuf Technol 68:1949–1965
51. Wu YJ, Yang H, Sun ZC, Fan XG (2006) Simulation on influence of local loading conditions on material flow during rib-web component forming. China Mech Eng 17(S1):12–15 (in Chinese)
52. Sun ZC, Yang H (2008) Characteristic of large-scale and complex rib-web components isothermal local loading forming. In: Yang DY, Kim YH, Park CH (eds) Proceedings of the 9th International Conference on Technology of Plasticity (ICTP2008). Korean Society for Technology of Plasticity, Seoul, pp 1585–1590
53. Zhang DW, Yang H (2013) Numerical study of the friction effects on the metal flow under local loading way. Int J Adv Manuf Technol 68:1339–1350
54. Wold S, Martens H, Wold H (1983) The multivariate calibration problem in chemistry solved by the PLS method. Lect Notes Math 97:286–293
55. Wold S, Sjöström M, Eriksson L (2001) PLS-regression: a basic tool of chemometrics. Chemom Intell Lab Syst 58:109–130
56. Zhang DW, Yang H (2014) Development of transition condition for the region with variable-thickness in isothermal local loading process. Trans Nonferrous Met Soc China 24(4):1101–1108
57. Zhang DW, Yang H (2015) Fast analysis on metal flow in isothermal local loading process for multi-ribs component using slab method. Int J Adv Manuf Technol 79:1805–1820
58. Altan T, Oh SI, Gegel HL (1983) Metal forming: fundamentals and application. American Society for Metals, Metal Park
59. Lange K (1985) Handbook of metal forming. McGraw-Hill, New York
60. Groche P, Müller C, Stahlmann J, Zang S (2013) Mechanical conditions in bulk metal forming tribometers—Part one. Tribol Int 62:223–231
61. Petersen SB, Martins PAF, Bay N (1997) Friction in bulk metal forming: a general friction model vs. the law of constant friction. J Mater Process Technol 66:186–194
62. Ghassemali E, Tan MJ, Jarfors AEW, Lim SCV (2013) Progressive microforming process: towards the mass production of micro-parts using sheet metal. Int J Adv Manuf Technol 66:611–621
63. Huang MN, Tzou GY (2002) Study on compression forming of a rotating disk considering hybrid friction. J Mater Process Technol 125–126:421–426
64. Kobayashi S, Oh SI, Altan T (1989) Metal forming and the finite-element method. Oxford University Press, New York
65. Tan X (2002) Comparisons of friction models in bulk metal forming. Tribol Int 35:385–393
66. Zhang Q, Felder E, Bruschi S (2009) Evaluation of friction condition in cold forging by using T-shape compression test. J Mater Process Technol 209:5720–5729
67. Gavrus A, Francillette H, Pham DT (2012) An optimal forward extrusion device proposed for numerical and experiment analysis of materials tribological properties corresponding to bulk forming processes. Tribol Int 47:105–121
68. Joun MS, Moon HG, Choi IS, Lee MC, Jun BY (2009) Effects of friction laws on metal forming processes. Tribol Int 42:311–319
69. Zhang DW, Ou HA Relationship between friction parameters in Coulomb-Tresca friction model for bulk metal forming. Tribol Int 95:13–18
70. Zhang DW, Yang H, Li HW, Fan XG (2012) Friction factor evaluation by FEM and experiment for TA15 titanium alloy in isothermal forming process. Int J Adv Manuf Technol 60:527–536
71. Zhang DW (2017) Friction and influence in FEM simulation of local loading process for titanium alloy rib-web component. Aeronaut Manuf Technol 4:34–41 (in Chinese)
72. Zhang DW, Yang H, Sun ZC, Fan XG (2010) A New FE Modeling method for isothermal local loading process of large-scale complex titanium alloy components based on DEFORM-3D. In: Frederic Barlat F, Moon YH, Lee MG (eds) AIP Conference Proceedings, vol 1252. American Institute of Physics, Melville, New York, pp 439–446
73. Gao PF, Yang H, Fan XG (2014) Quantitative analysis of the material flow in transitional region during isothermal local loading forming of Ti-alloy rib-web component. Int J Adv Manuf Technol 75:1339–1347
74. Gao PF, Yang H, Fan XG, Lei P (2015) Forming defects control in transitional region during isothermal local loading of Ti-alloy rib-web component. Int J Adv Manuf Technol 76:857–868
75. Malayappan S, Narayanasamy R (2004) An experiment analysis of upset forging of aluminium cylindrical billets considering the dissimilar friction conditions at flat die surface. Int J Adv Manuf Technol 23:636–643
76. Shan DB, Zhang YQ, Wang Y, Xu FC, XU WC, Lü Y (2006) Defect analysis of complex-shape aluminum alloy forging. Trans Nonferrous Met Soc China 16(S3):1574–1579
77. Zhang DW, Yang H, Sun ZC, Fan XG (2012) Deformation behavior under die partitioning boundary during titanium alloy large-scale rib-web component forming by isothermal local loading. In: Zhou L, Chang H, Lu YF, Xu DS (eds) Proceedings of the 12th World Conference on Titanium. Science Press, Beijing, pp 328–332
78. Sun ZC, Yang H, Sun NG (2009) Simulation on local loading partition during titanium bulkhead isothermal forming process. J Plast Eng 16(1):138–143 (in Chinese)
79. Zhang DW, Yang H, Sun ZC, Fan XG (2012) Deformation behavior of variable-thickness region of billet in rib-web component isothermal local loading process. Int J Adv Manuf Technol 63:1–12

80. Sun ZC, Yang H ((2008)) Mechanism of unequal deformation during large-scale complex integral component isothermal local loading forming. Steel Res Int 79(Special 1):601–608
81. Sun ZC, Yang H, Sun NG (2012) Effects of parameters on inhomogeneous deformation and damage in isothermal local loading forming of Ti-alloy component. J Mater Eng Perform 21(3):313–323
82. Sun ZC, Yang H (2009) Microstructure and mechanical properties of TA15 titanium alloy under multi-step local loading forming. Mater Sci Eng A 523:184–192
83. Fan XG, Gao PF, Yang H (2011) Microstructure evolution of the transitional region in isothermal local loading of TA15 titanium alloy. Mater Sci Eng A 528:2694–2703
84. Zhang DW, Yang H (2013) Preform design for large-scale bulkhead of TA15 titanium alloy based on local loading features. Int J Adv Manuf Technol 67:2551–2562
85. Wei K, Yang H, Fan XG, Gao PF (2015) Unequal thickness billet design for large-scale titanium alloy rib-web components under isothermal closed-die forging. Int J Adv Manuf Technol 81:729–744
86. Sun ZC, Yang H (2009) Analysis on process and forming defects of large-scale complex integral component isothermal local loading. Mater Sci Forum 614:117–122
87. Zhang DW, Yang H (2014) Distribution of metal flowing into unloaded area in the local loading process of titanium alloy rib-web component. Rare Metal Mater Eng 43(2):296–300
88. Gao PF, Liu ZF, Lei ZN (2017) Deformation characteristics of transitional region during local loading forming of Ti-alloy rib-web component on the double-action process. Int J Adv Manuf Technol 93:599–567
89. Gao PF, Yang H, Fan XG, Lei PH (2015) Quick prediction of the folding defect in transitional region during isothermal local loading forming of titanium alloy large-scale rib-web component based on folding index. J Mater Process Technol 219:101–111
90. Gao PF, Yang H, Fan XG, Lei P (2015) Forming limit of local loading forming of Ti-alloy large-scale rib-web components considering defects in the transitional region. Int J Adv Manuf Technol 80:1015–1026
91. Gao PF, Yang H, Fan XG, Lei PH, Meng M (2014) Prediction of folding defect in transitional region during local loading forming of titanium alloy large-scale rib-web component. Procedia Eng 81: 528–533
92. Park JJ, Hwang HS (2007) Preform design for precision forging of an asymmetric rib-web type component. J Mater Process Technol 187–188:595–599
93. Zhang DW, Yang H, Sun ZC, Fan XG (2011) Influences of fillet radius and draft angle on the local loading process of titanium alloy T-shaped components. Trans Nonferrous Metals Soc China 21(12): 2693–2074
94. Gao PF, Li XD, Yang H, Fan XG, Lei ZN (2017) Influence of die parameters on the deformation inhomogeneity of transitional region during local loading forming of Ti-alloy rib-web component. Int J Adv Manuf Technol 90:2109–2119
95. Gao PF, Li XD, Yang H, Fan XG, Lei ZN (2017) Improving the process forming limit considering forming defects in the transitional region in local loading forming of Ti-alloy rib-web components. Chin J Aeronaut 30(3):1270–1280
96. Sun ZC, Yang H (2009) Forming quality of titanium alloy large-scale integral components isothermal local loading. Arab J Sci Eng 34(1C):35–45
97. Wei K, Fan XG, Zhan M, Yang H, Gao PF (2017) Improving the deformation homogeneity of the transitional region in local loading forming of Ti-alloy rib-web component by optimizing unequal-thickness billet. Int J Adv Manuf Technol 92:4017–4029
98. Wei K, Zhan M, Fan XG, Yang H, Gao PF, Meng M (2018) Unequal-thickness billet optimization in transitional region during isothermal local loading forming of Ti-alloy rib-web component using response surface method. Chin J Aeronaut 31(4):845–859
99. Fan XG, Yang H, Sun ZC, Zhang DW (2010) Effect of deformation inhomogeneity on the microstructure and mechanical properties of large-scale rib-web component of titanium alloy under local loading forming. Mater Sci Eng A 527:5391–5399